

# Analysis of a self-contained motion capture garment for e-textiles

Robert Lewis

Thesis submitted to the Faculty of the  
Virginia Polytechnic Institute and State University  
in partial fulfillment of the requirements for the degree of

Master of Science  
in  
Computer Engineering

Thomas L. Martin, Co-Chair

Mark Jones, Co-Chair

Peter Athanas

May 4, 2011

Blacksburg, Virginia

Keywords: E-textiles, Wearable Computing, Inertial Measurement Units

Copyright 2011, Robert Lewis

# Analysis of a self-contained motion capture garment for e-textiles

Robert Lewis

## ABSTRACT

*Wearable computers and e-textiles are becoming increasingly widespread in today's society. Motion capture is one of the many potential applications for on-body electronic systems. Previous work has been performed at Virginia Tech's E-textiles Laboratory to design a framework for a self-contained loose fit motion capture system. This system gathers information from sensors distributed throughout the body on a "smart" garment. This thesis presents the hardware and software components of the framework, along with improvements made to it. This thesis also presents an analysis of both the on-body and off-body network communication to determine how many sensors can be supported on the garment at a given time. Finally, this thesis presents a method for determining the accuracy of the smart garment and shows how it compares against a commercially available motion capture system.*

# Acknowledgements

The work shown in this thesis would not have been accomplished without the help and support of a lot of people. For those who are not mentioned specifically, thank you.

I would like to thank my advisor, Dr. Tom Martin, for his advice, support, and guidance through my entire graduate career. Without his help I could not have succeeded.

I would like to thank my co-advisor, Dr. Mark Jones, for his helpful critiques and guidance throughout the entire process.

I would like to thank Dr. Peter Athanas for serving on my committee.

I would like to thank Dr. Thurmon Lockhart, Xiaoyue Zhang, and Rahul Songra for their help and allowing the use of the motion capture equipment to perform many of the tests in this thesis.

I would like to thank Jacob Simmons, David Uliana, and Sudhanshu Mishra for their efforts in helping me work through problems encountered during this process.

I would like to thank Kara Baumann for designing the e-textiles garment, and for helping when issues in the garment arose.

I would like to thank Bob Lineberry for his help with the printed circuit board design and soldering tips.

I would like to thank Lalleh Rafeei for all the help she has given me through this process, and for making sure I never gave up along the way.

I would like to thank my friends for the support they gave me through this entire process.

And above all, I would like to dedicate this thesis to my parents Mark and Joyce Lewis. I would never have been given this opportunity in life without their help. It is because of their constant guidance and encouragement that has led me to where I am today.

This material is based upon work supported by the National Science Foundation under Grant No. CNS-0447741. Any opinions, findings, and conclusions or recommendations expressed in this material are those of the author and do not necessarily reflect the views of the National Science Foundation(NSF).

# Contents

|          |  |           |
|----------|--|-----------|
| <b>1</b> | <b>Introduction</b>                                    | <b>1</b>  |
| 1.1      | Motivation . . . . .                                   | 1         |
| 1.2      | Contributions . . . . .                                | 2         |
| 1.3      | Thesis Organization . . . . .                          | 2         |
| <b>2</b> | <b>Related Work</b>                                    | <b>3</b>  |
| 2.1      | Motion Capture Systems . . . . .                       | 3         |
| 2.2      | Previous E-textile Research at Virginia Tech . . . . . | 4         |
| <b>3</b> | <b>Overview of Hardware and Software</b>               | <b>6</b>  |
| 3.1      | Hardware Overview . . . . .                            | 6         |
| 3.2      | Hardware Modifications . . . . .                       | 7         |
| 3.2.1    | Sensors . . . . .                                      | 7         |
| 3.2.2    | Garment . . . . .                                      | 8         |
| 3.3      | Compass Calibration . . . . .                          | 10        |
| 3.4      | Software Overview . . . . .                            | 11        |
| 3.4.1    | Tier 1 . . . . .                                       | 11        |
| 3.4.2    | Tier 2 . . . . .                                       | 11        |
| 3.5      | Software Modifications . . . . .                       | 12        |
| 3.5.1    | Packet Structure . . . . .                             | 12        |
| <b>4</b> | <b>Networking</b>                                      | <b>14</b> |
| 4.1      | Networking Overview . . . . .                          | 14        |
| 4.2      | On-body Communication . . . . .                        | 14        |
| 4.2.1    | Current Setup . . . . .                                | 17        |
| 4.2.2    | Reducing Packet Size . . . . .                         | 18        |
| 4.3      | Off-body Communication . . . . .                       | 19        |

|          |  |           |
|----------|--|-----------|
| 4.3.1    | Wired vs Bluetooth . . . . .                   | 19        |
| 4.4      | Potential Bottleneck . . . . .                 | 20        |
| <b>5</b> | <b>Results</b>                                 | <b>21</b> |
| 5.1      | Motivation and Methodology . . . . .           | 21        |
| 5.2      | Comparing Motion Capture System Data . . . . . | 24        |
| 5.2.1    | Initial Body Structure Analysis . . . . .      | 25        |
| 5.2.2    | Data Mapping and Comparison . . . . .          | 28        |
| 5.3      | Test Subject Results . . . . .                 | 30        |
| 5.3.1    | Overall Error Analysis . . . . .               | 31        |
| 5.3.2    | Sources of Error . . . . .                     | 33        |
| 5.3.3    | Hard-iron Error . . . . .                      | 39        |
| 5.3.4    | Segment and Joint Angle Error . . . . .        | 43        |
| 5.3.5    | Analyzing Marker Position . . . . .            | 46        |
| <b>6</b> | <b>Conclusions and Future Work</b>             | <b>49</b> |
| 6.1      | Conclusion . . . . .                           | 49        |
| 6.2      | Future Work . . . . .                          | 50        |
| <b>A</b> | <b>Result Tables</b>                           | <b>53</b> |

# List of Figures

|      |  |    |
|------|--|----|
| 3.1  | Representation of the two-tier system used in this thesis . . . . .  | 7  |
| 3.2  | The upper body e-textiles garment used in this thesis . . . . .  | 9  |
| 3.3  | Packet Structure sent by Tier 1 sensor . . . . .   | 13 |
| 4.1  | Tier 1 sensor packets being transmitted on-body via I <sup>2</sup> C . . . . .   | 15 |
| 4.2  | Closeup of Tier 1 sensor packets . . . . .   | 15 |
| 4.3  | Frequency vs. sensors supported with 17-byte packets . . . . .   | 17 |
| 4.4  | Frequency vs. sensors gained by reducing packet size 2 bytes . . . . .   | 18 |
| 4.5  | Frequency vs. sensors supported when streaming data in real time off-body . . . . .  | 20 |
| 5.1  | Placement of optical markers on body . . . . .   | 22 |
| 5.2  | Left arm out including where the optical markers would be located on the garment . . . . .   | 23 |
| 5.3  | T-position including where the optical markers would be located on the garment . . . . .   | 23 |
| 5.4  | Finding the quaternion which maps the garment vector to the optical vector . . . . .   | 25 |
| 5.5  | Location of the six segments whose length are initially taken . . . . .  | 26 |
| 5.6  | Finding the torso's orientation given three marker positions . . . . .   | 27 |
| 5.7  | Mean and maximum average error and STD for marker positions across all test subjects and all tests . . . . .   | 32 |
| 5.8  | Mean and maximum average error and STD angles for segment angles across all test subjects and all tests. The torso error represents the angle which the systems differ by at the midpoint between the shoulders. . . . . | 33 |
| 5.9  | Average position error in Test #8, right arm bend, for all five subjects . . . . .   | 35 |
| 5.10 | Average position error in Test #8, right arm bend, using subjectE's improved torso location . . . . .  | 36 |
| 5.11 | Absolute position of the torso over time for SubjectE in Test #8, right arm bend . . . . .   | 36 |
| 5.12 | Left elbow bend highlighting hard-iron error . . . . .   | 37 |
| 5.13 | Difference in marker position between systems at the left wrist during a left arm bend . . . . .   | 37 |

|      |   |    |
|------|---|----|
| 5.14 | Average segment angle error in Test #4, right arm bend, for all five subjects. STD is larger in the right arm due to hard-iron error. The torso error represents the angle which the systems differ by at the midpoint between the shoulders. . . . . | 38 |
| 5.15 | Attachment of sensors to a ruler for hard-iron error visualization . . . . .  | 39 |
| 5.16 | Hard-iron error of two compasses outdoors . . . . .   | 41 |
| 5.17 | Hard-iron error of two compasses inside a building . . . . .  | 41 |
| 5.18 | Hard-iron error of two compasses inside a building at a different location . . . . .  | 42 |
| 5.19 | Hard-iron error of two compasses in subject testing room . . . . .  | 42 |
| 5.20 | Average segment angle error for each test subjects across all tests. The torso error represents the angle which the systems differ by at the midpoint between the shoulders. . . . .  | 45 |
| 5.21 | Average joint angle error for each test subjects across all tests . . . . .   | 45 |
| 5.22 | Average position error in Test #1, left arm out, for all five subjects . . . . .  | 47 |
| 5.23 | Average position error across all tests for each subject. Order of the x-axis has changed to highlight symmetry between the body . . . . .  | 47 |
| 5.24 | SubjectA's right side upper and lower limb error in Test #1, left arm out . . . . .   | 48 |

# List of Tables

|      |   |    |
|------|---|----|
| 3.1  | Major components found on a Tier 1 node . . . . .   | 7  |
| 4.1  | Minimum ideal and actual measured times for Tier 1 I <sup>2</sup> C communication . . . . .       | 16 |
| 4.2  | Delays associated with the I <sup>2</sup> C software running on the 32MHz PIC processor . . . . . | 16 |
| 5.1  | Summary of the eight tests each user is instructed to perform . . . . .                           | 24 |
| 5.2  | Maximum range of error between two compasses in various locations . . . . .                       | 40 |
| A.1  | Mean and STD error of distance for each marker between suits for SubjectA . . . . .               | 53 |
| A.2  | Mean and STD error of distance for each marker between suits for SubjectB . . . . .               | 53 |
| A.3  | Mean and STD error of distance for each marker between suits for SubjectC . . . . .               | 54 |
| A.4  | Mean and STD error of distance for each marker between suits for SubjectD . . . . .               | 54 |
| A.5  | Mean and STD error of distance for each marker between suits for SubjectE . . . . .               | 54 |
| A.6  | Mean and STD angle error at each segment of the body for SubjectA . . . . .                       | 55 |
| A.7  | Mean and STD angle error at each segment of the body for SubjectB . . . . .                       | 55 |
| A.8  | Mean and STD angle error at each segment of the body for SubjectC . . . . .                       | 55 |
| A.9  | Mean and STD angle error at each segment of the body for SubjectD . . . . .                       | 56 |
| A.10 | Mean and STD angle error at each segment of the body for SubjectE . . . . .                       | 56 |
| A.11 | Mean and STD angle error at each joint of the body for SubjectA . . . . .                         | 57 |
| A.12 | Mean and STD angle error at each joint of the body for SubjectB . . . . .                         | 57 |
| A.13 | Mean and STD angle error at each joint of the body for SubjectC . . . . .                         | 57 |
| A.14 | Mean and STD angle error at each joint of the body for SubjectD . . . . .                         | 58 |
| A.15 | Mean and STD angle error at each joint of the body for SubjectE . . . . .                         | 58 |

# Chapter 1

## Introduction

### 1.1 Motivation

Electronic textiles (e-textiles) and wearable computing devices are becoming increasingly widespread in today's world. Most everyday devices, from cellphones to portable music players, are wearable computers that people depend on. With this technology becoming ubiquitous, research has gone into designing clothing with wearable computers in them. Virginia Tech's E-textiles Lab has previously designed a self-contained smart garment system [1]. This system is a framework which has been designed to capture and transmit inertial measurement data from segments of the body. This framework was built with customization in mind, allowing sensors to be placed on the body where needed [2]. With this framework in place, testing can begin to measure the accuracy of the self-contained garment.

Typical commercial systems use fasteners or elastic clothing to restrict movement of devices on the wearer, while also needing external hardware to capture the motion. In contrast, the smart garment system takes a different approach to capturing motion by being both self-contained and loose fitting. By being self-contained the garment can be used outside of laboratory settings, allowing the wearer to go anywhere while processing and storing data locally. By allowing the garment to be loose fitting, this technology can be miniaturized and placed ubiquitously. These properties help open up new avenues for motion capture technology to be applied.

## 1.2 Contributions

This thesis presents the design and analysis of a self-contained motion capture system with emphasis on a loose fit e-textiles garment. The loose fit and self-contained aspects of the garment afford for it to be used in situations not designed for by current motion capture systems. The design presented in this thesis makes improvements to the already created framework, allowing individual and overall body pose to be easily tracked. A method was also designed to test the accuracy of the smart garment's pose against that of a commercially used optical motion capture system that has been industry-tested for reliability.

## 1.3 Thesis Organization

This thesis is organized as follows. Chapter 2 outlines the background information needed to understand the research conducted in this paper. Chapter 3 describes both the hardware and software aspects needed to construct the self-contained garment. Chapter 4 describes the networking protocol used and how data is transmitted. Chapter 5 describes the results and analysis of the self-contained garment's performance compared to an industry grade system. Finally, Chapter 6 summarizes the contributions of this thesis and conclusions drawn from this research, and provides new approaches for attempting future work on this project.

# Chapter 2

## Related Work

This chapter outlines key topics that relate to this thesis. Several key concepts were leveraged to develop the smart garment system described in this thesis. This chapter gives an overview of motion capture systems and how their development relates to this work. This chapter then talks about previous projects completed in the E-textiles Research Laboratory and the evolution of the smart garment system.

### 2.1 Motion Capture Systems

Motion capture has been around since the early 1900s, starting with a technique called rotoscoping. Rotoscoping is performed by first capturing a live action scene. That scene is then played back frame-by-frame allowing the animator to retrace the scene onto paper to produce an animation. As time progressed, this technology advanced and gave way to alternative ways for animators and others to capture and manipulate human movement.

The motion capture technology used in this thesis leverages inertial measurement units (IMU). Typically these sensors consist of accelerometers and gyroscopes to determine their position and orientation. These sensors are then attached to segments of the body to track the segment's movement and orientation.

Currently there are a number of techniques used to capture human motion, each with their own benefits. Such techniques include computer vision algorithms, mechanical exoskeletons, and optics. These systems may integrate IMUs into their design, or choose to rely entirely on external tracking methods [3]. By relying on external methods to track human motion, these systems are generally more expensive and less portable.

Relatively inexpensive and highly mobile solutions for inertial motion capture have been demonstrated in applications ranging from gaming [4] to medical [5]. The XSens MVN Motion Capture suit is one successful commercial option that uses IMUs and magnetometers to track motion, however this system costs around \$60,000 to purchase [6].

A common issue with IMUs is that they drift over time. This measurement drift is a result of integrating raw acceleration or angular velocity to determine position and joint angles on the body. These integration errors are small, but compound and accumulate over time. External methods can be used to correct for this drift, such as using optical markers [7]. While this does correct measurement drift, it adds external components and causes the system to become less portable. Our implementation approach is to bundle a slow, but highly accurate, sensor with the IMU which can measure absolute orientation. This approach keeps all hardware local to the body while also limiting possible drift due to accumulated error. A similar design which tracks orientation angles instead of position estimates has been demonstrated to be successful [8].

There has been previous work done with inertial measurement systems to try and reduce the impact of these issues, but usually does so at the expense of increased constraints in motion or narrowed scope. The sportSemble system developed at MIT uses a hardware configuration similar to the one presented in this thesis to track the movement of baseball players. However, this system focuses on the biomedical effects of short, intense bursts of activity on specific segments of the body rather than full-body motion capture over long periods of time [5]. Other experiments have focused exclusively on gait detection [9] or gesture recognition [10].

The design presented in this thesis differs from similar self-contained motion capture suit implementations, such as the Xsens MVN suit. Our design makes use of e-textiles to weave all communication wires directly into the fabric of the garment, allowing the motion capture system to more closely resemble putting on and wearing actual clothing. The garment presented in this thesis differs by being a loose fit item, removing the need for sensors to be strapped to the body as required by other motion capture systems.

## **2.2 Previous E-textile Research at Virginia Tech**

The Virginia Tech E-textile Laboratory has done research for a past number of years in developing a “smart” motion capture garment. This garment has characteristics of being both loose-fitting and self-contained. These characteristics afford the smart garment to be used in situations where conventional motion capture would not be desirable. While the loose fit of the garment means some loss of precision in tracking position,

this garment has a huge advantage of being worn like traditional clothing with no need for external data capture. Potential applications for this garment include gait analysis and movement rehabilitation.

This research performed at Virginia Tech has led to a framework in how to design both the software and hardware components. Earlier research performed by Quirk [11] has shown the feasibility of producing e-textiles with conductive material capable of transmitting signals through clothing. Virginia Tech is capable of producing these garments in-house with an automated loom.

The first version of the smart garment consisted of a pair of pants with embedded wires in them. These pants were equipped with on-body accelerometers and gyroscopes to capture movement of the body. This data was then compared with expected results from a simulated environment [1]. Later research focused on activity recognition, using algorithms to classify the on-body accelerometer and gyroscope readings [12]. The processed data was then compared against a list of known activities to determine which was most likely being performed. Most recently a framework for the smart garment has been developed. This framework describes both the hardware and software components needed to gather information from the body [2]. This framework has also upgraded the sensors used, using gyroscopes and digital compasses to detect the wearer's pose without drift.

During these iterations the garment was converted into a full body jumpsuit. Additional features were also added to the garment. USB-like connectors allowed sensors to be dynamically placed on the garment. A central processor, the Verdex 400xmbt motherboard from Gumstix, was also added which allowed for local processing of data and off-body communication to a nearby PC via serial or Bluetooth connection. The work performed in [13] established a two-tiered network for on-body communication. This network allowed Tier 1 sensors to collect and report their readings to a central Tier 2 processor, the Verdex 400xmbt, for data processing.

The work in this thesis builds off of the framework created by Simmons [2]. The framework is to be applied to a newly constructed garment, one that is more versatile and built for prototyping. This framework is also sought to be extended upon, making improvements at the software level to more accurately track the pose of the garment. Finally, the garment is to be compared against a commercially available motion capture system to test its accuracy.

## Chapter 3

# Overview of Hardware and Software

### 3.1 Hardware Overview

This thesis uses custom designed hardware on a garment for self-contained motion capture. The hardware configuration used is a two-tier system that is interconnected using a wired network that is woven or sewn directly into the fabric. Both tiers reside on the clothing and use the I<sup>2</sup>C protocol to communicate via the on-body network. This framework was developed in a previous Virginia Tech E-textiles research project by Chong [13]. For the application described in this thesis, our system makes use of many Tier 1 sensors and only one Tier 2 processor. The hardware found at both the Tier 1 and Tier 2 levels is the same used in Simmon's thesis [2]. Figure 3.1 gives a visual representation of how the nodes are connected together to form the two-tier system. The rectangular blocks represent particular PCB nodes in the system, while the lines represent communication between those nodes. The *Timer* node is a special type of Tier 1 sensor that has been added since Simmon's thesis, and will be discussed in following section. All other items will be discussed in the following paragraphs.

The Tier 1 sensors used in this thesis are relatively simplistic sensors whose task is to acquire and transmit inertial data to the Tier 2 level. Table 3.1 lists the major components found on every Tier 1 node. These components all operate at the same voltage, 3.3v, to keep the circuit design as simple as possible. Each Tier 1 node is placed at a designated spot on the body and transmits its measured acceleration, rotation, and orientation along all three axes at a system-specified frequency to its onboard microprocessor. The microprocessor then packets this data and transmits it along the on-body network to the Tier 2 level.

The Tier 2 processor serves as the central processing unit for our system. The processor found here is the Verdex 400xmbt motherboard from Gumstix, the same processor successfully used in earlier versions of the garment at the Virginia Tech E-textiles Lab. The Verdex 400xmbt runs a full Linux operating system and can be interfaced by either Bluetooth or wired serial. Each packet of data transmitted by a Tier 1 sensor is recorded at the Tier 2 level, that is then processed. This processed data can either be stored locally or transmitted off the suit via wired serial or Bluetooth to a standard personal computer for further data analysis. The Gumstix has an additional PCB attached to it, designed by a previous student in the Virginia Tech E-textiles Lab, that converts I<sup>2</sup>C data into serial data. This additional PCB is connected to the on-body network, allowing the Gumstix to listen to data being transmitted by the Tier 1 sensors.

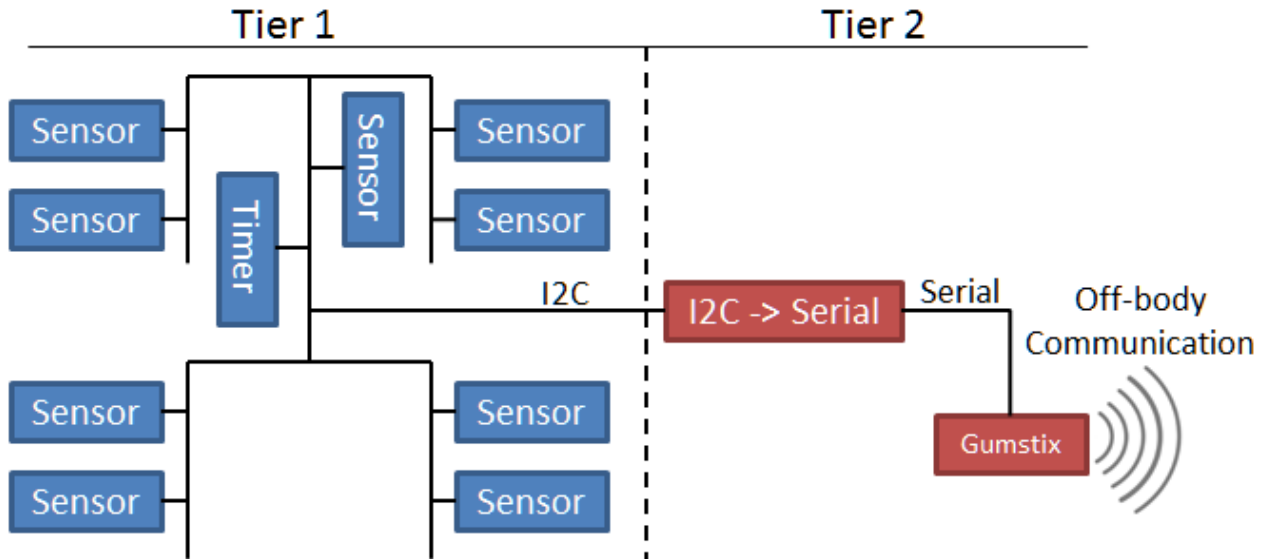


Figure 3.1: Representation of the two-tier system used in this thesis

| Component       | Amount | Axis | Communication    | Part Number |
|-----------------|--------|------|------------------|-------------|
| Microprocessor  | 1      | –    | –                | PIC18F6722  |
| Accelerometer   | 1      | 3    | I <sup>2</sup> C | ADXL345     |
| Gyroscope       | 2      | 2    | Analog           | LPR530AL    |
| Digital Compass | 1      | 3    | I <sup>2</sup> C | HMC6343     |

Table 3.1: Major components found on a Tier 1 node

## 3.2 Hardware Modifications

### 3.2.1 Sensors

There have been two sensor hardware modifications applied to Simmon's thesis. The first involves the gyroscopes as it was found that the ones previously used had a flaw in the circuit design. The circuit contained

high-pass filters on the analog data lines, causing incorrect data to be reported when the gyroscope moved at a slow rate. The manufacture's website has since acknowledged this flaw and all gyroscopes used in this thesis have been corrected [14].

The second modification comes from the addition of an extra Tier 1 sensor. This sensor does not utilize any of the inertial sensors found on its PCB, as it is used solely for its microprocessor and I<sup>2</sup>C communication ability. This additional sensor has been included as a result of a software design change. The sensor is used as a global synchronization timer, controlling the frequency at which data is sent across the on-body network.

### **3.2.2 Garment**

The garment used in the application for this thesis is not the same one used in previously e-textiles research projects. This new garment has been designed from the ground up by a fellow researcher, Kara Baumann, who works in the E-textiles Research Laboratory. This garment has several advantages over the previous one allowing a wider variety of sized people to fit comfortably in, a more appropriate fitting to the user, and rapid prototyping capability due to the garment allowing dynamic placement of sensors. Once completed, the garment will be a two piece that connects together at the waist to form an identical on-body network found on the previously used garment.

Figure 3.2 shows the completed top half of the garment. At the time of performing the experiments in this thesis, this was the only completed portion of the garment. Grommets are laced throughout the garment allowing sensor fabric, the green fabric shown in the figure, to be dynamically placed. The sensor fabric has wires and sensor connectors sewn into them allowing Tier 1 sensors to be added or removed when needed. The garment also contains elastic straps in various places, allowing the wearer to be properly fitted.



Figure 3.2: The upper body e-textiles garment used in this thesis

### 3.3 Compass Calibration

The HMC6343 digital compass used in this thesis relies on internal magneto-resistive magnetometers and MEMS accelerometers to detect heading, pitch, and roll [15]. The magnetometers are susceptible to changes in the magnetic field and must be calibrated in order to ensure proper readings. There are two types of magnetic error that lead to improper readings, hard-iron and variation, both of which can be corrected for by the microprocessor present in the digital compass. The National Geophysical Data Center, NGDC, was used to find information pertaining to Blacksburg Virginia, such as the earth's total field and variation angle [16]. This information will aid in correcting these two types of errors.

Hard-iron, or deviation, errors form an arc graphically when measuring the reported heading versus the expected heading while sweeping through 360 degrees parallel to the earth's surface, or z-axis. This error theoretically appears as a symmetric sine wave with no error at 0 and 180 degrees. It is also possible for the error to appear as a non-symmetric wave, or one that only has negative or positive heading error [17]. Hard-iron error is a result of ferrous material present in a fixed position relative to the digital compass, measuring in a non-clean magnetic field environment, such as inside a building, or from having performed the hard-iron calibration in a non-clean magnetic field environment. A magnetically clean environment is described as being an area with no nearby objects which could perturb the earth's magnetic field [18]. In order to correct for this problem the compass must be relocated outdoors where the magnetic field is the same strength as the earth's. The strength of the earth's magnetic field changes based on location, so the reported value supplied by the NGDC was used for reference in finding a suitable area to calibrate. The HMC6343 datasheet details the steps that need to be taken in order to perform the hard-iron calibration routine. This routine consists of rotating the compass about the y-axis followed by the z-axis over the course of about a minute. Doing so allows the compass to sample the surrounding magnetic field and update the magnetometer offset values stored in its EEPROM.

Variation, or declination, is the difference between true north and magnetic north. Since the angle between these two versions of north varies based on location the degree difference found on the NGDC site must be programmed into the EEPROM of the device, where negative offsets shift the heading westward and positive offsets shift the heading eastward. When the digital compass samples data it will apply the variation angle to its measured heading in order to produce an accurate result [19].

## 3.4 Software Overview

### 3.4.1 Tier 1

There are a total of ten Tier 1 nodes on the garment. Nine of the nodes collect inertial data while the tenth node is used as a system synchronization timer. The synchronization node sends a message at a specified frequency along the on-body network to notify the Tier 1 sensors when to begin collecting and transmitting data. The synchronization sensor is important because of drift that exists in hardware timers. With this setup all sensors will drift together by the same amount, the drift of the synchronization node.

Each Tier 1 microprocessor is programmable using the raised header found on its PCB. A PICkit programmer can be attached to the header, allowing software to be downloaded to its microprocessor using the MPLAB software suite. This ability not only allows the sensors to be reprogrammed for various applications, but also makes debugging easier.

When the suit is first powered on, the data-collecting sensors initialize their on-board accelerometer and digital compass, followed by setting themselves to slave I<sup>2</sup>C mode. In this mode the sensors will wait until a message is seen along the network from the synchronization timer. Once seen, the data-collecting sensors will read up-to-date data from their accelerometer, gyroscopes, and digital compass. They will then switch over to master I<sup>2</sup>C mode, transmit their data across the network, and finally switch back to slave I<sup>2</sup>C mode. This process will occur across all nine data-collecting sensors with bit collision detection enabled, to ensure that each sensor is successfully able to send.

The packets sent by a Tier 1 sensor alternate between *full packets* and *half packets*. A full packet, or update, is described as a sensor sending its identification, acceleration, gyroscope, and compass information across the on-body network. The half packet differs from the full packet by excluding the sensor's compass information. The reason two packet types exist is because the digital compass operates at a maximum frequency of 10Hz. By reducing the packet size on non-compass updates, a higher throughput can be achieved along the on-body network. The packet structure sent by a Tier 1 sensor is described in greater detail in the following section.

### 3.4.2 Tier 2

Data transmitted by the Tier 1 sensor is then received by the Tier 2 node. This node monitors all traffic along the network and is where the major processing for this system is performed. The two main applications used

for data-collection and processing are called *tty\_relay*, and *motion\_capture*. The first application, *tty\_relay*, is a simplistic one that streams the unmodified packets received from the Tier 1 sensors to either a file or across Bluetooth to a personal computer. This is valuable for seeing the type of information being captured at each point on the body and debugging for errors. The second application, *motion\_capture*, acts as it did in Simmon’s thesis, with a small but important modification. The heading, pitch, and roll read from a Tier 1 sensor’s compass is immediately converted into a quaternion before any data is combined, and any further processing is performed strictly in quaternion space. Once the compass data has been converted into its quaternion equivalent the gyroscope data is then appended, resulting in a final quaternion that represents the current orientation of that sensor. The resulting data is then either saved to a file or transmitted to a personal computer via Bluetooth.

There are two reasons for representing the data as a quaternion instead of Euler angles. The first advantage is that Euler angles describe three separate rotations, thus suffering from gimbal lock, while quaternions describe rotation using a single axis and angle. The second advantage is that it is easier to filter the data as a quaternion because the data does not consist of independent variables. An easy example to help illustrate the filtering problem would be to imagine a starting compass position, in degrees, at 0 heading, 89 pitch, and 0 roll. The compass then moves to the position, also in degrees, 180 heading, 89 pitch, and 180 roll. In Euler space it appears that heading and roll have changed drastically and pitch has remained the same, while the quaternion equivalent would have detected a two degree rotation mapping the first compass position into the second.

## 3.5 Software Modifications

### 3.5.1 Packet Structure

The packet structure at the Tier 1 level has been slightly modified from that in Simmon’s thesis. The addition of a global synchronization timer means the last byte, *packet count*, can be removed, resulting in the revised packet structure shown in Figure 3.3. The revised packet contains 17 bytes on a full update and 11 bytes on a half update.

The Tier 2 processor now keeps an internal *packet count* record that increments when the synchronization timer transmits on the network. This is done not only to increase throughput along the on-body network, but also to verify Tier 1 sensor integrity. The Tier 2 processor is able to see how many Tier 1 sensors have

sent data between synchronization pulses and determine if there is a problem collecting data at any limb.

Figure 3.3 is broken up into four groups, by color. Most of the data consists of two-byte pairs, labeled either LOW or UPP for the lower and upper byte, respectively. The first group is self-explanatory and simply contains the sensor's identification value. The second group of data, the gyroscope, needs four bytes to store each of its three axes; this is because each axis consists of 10 bits of data. In order to accommodate this length the lower 8 bits from each axis are placed into G<sub>x</sub>, G<sub>y</sub>, and G<sub>z</sub>, while the remaining 2 bits from each axis are combined and right-aligned to make up the fourth byte, G. This method only wastes 2 bits at the upper end of the G byte. The third group is for the acceleration and contains two-byte pairs for each of the three axes with the upper byte coming first followed by its respective lower byte. Lastly the fourth group is for the compass data. This group only exists on full updates and contains the 2 byte pairs for heading, pitch, and roll.

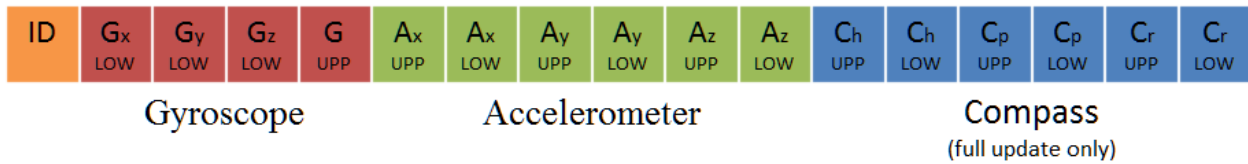


Figure 3.3: Packet Structure sent by Tier 1 sensor

# Chapter 4

## Networking

### 4.1 Networking Overview

The networking aspect of this system is the backbone of the garment. The network's capabilities and limitations define how the garment may be used. This chapter defines those limitations and illustrates how many sensors the suit can support when running given a specific frequency.

### 4.2 On-body Communication

On-body communication is defined as the communication of the Tier 1 sensors to the Tier 2 node. This communication, as discussed previously, uses the I<sup>2</sup>C protocol operating in fast mode at 400KHz. The Philips Semiconductors' specification datasheet lists the ideal minimum timing values required to guarantee correct operation of the protocol [20]. Table 4.1 shows a subset of these timing values applicable to the application presented in this thesis. Three terms,  $t_{byte\_buf}$ ,  $t_{su;addr}$ , and  $t_{data;stop}$  not found in the I<sup>2</sup>C specification datasheet have been added to this table to make generalizing a set of equations easier. These specified timing values define the maximum throughput which can be obtained by the Tier 1 sensors.

In addition, an oscilloscope was attached to the on-body network to measure the actual timing values of the Tier 1 sensors shown in the last column of Table 4.1. These timing values are dictated both by the hardware and the design decisions made in software. Figure 4.1 shows a capture of two Tier 1 sensors sending their packets across the on-body network along with the global synchronization pulse. Figure 4.2 is a zoomed in

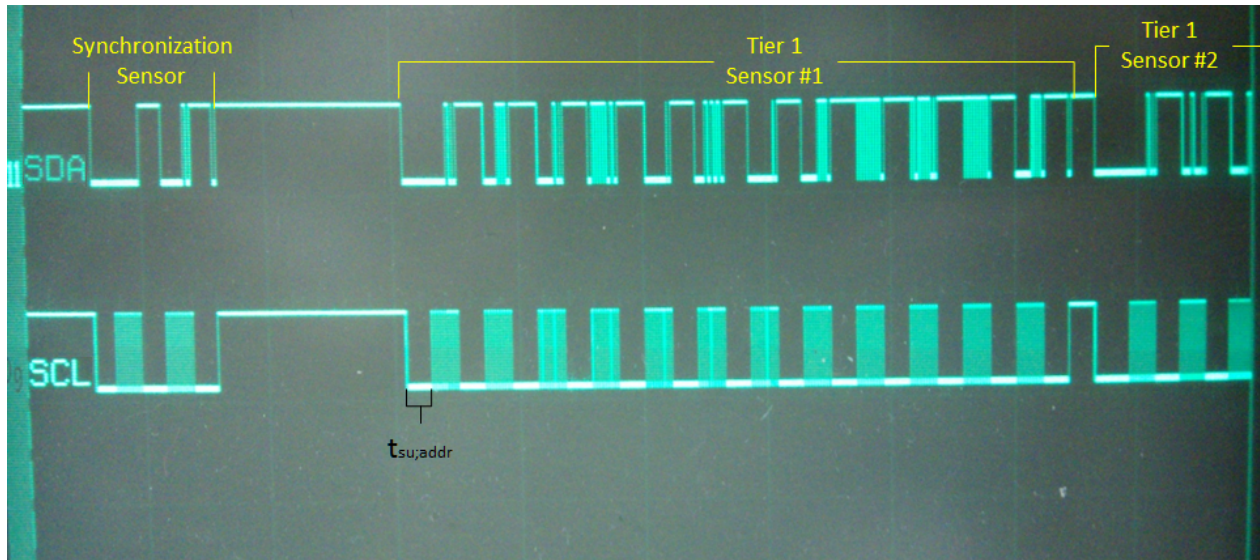


Figure 4.1: Tier 1 sensor packets being transmitted on-body via I<sup>2</sup>C

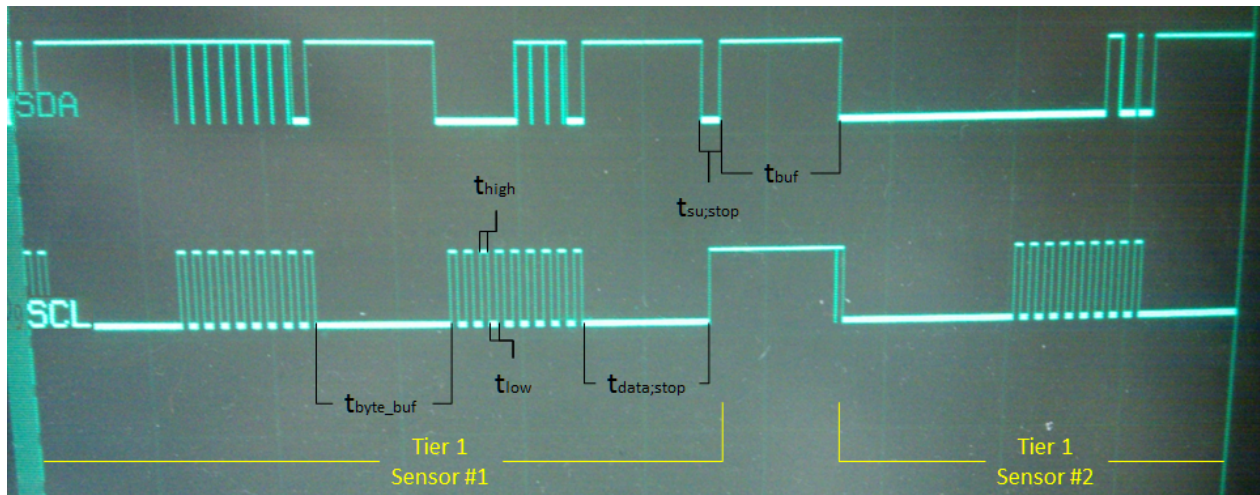


Figure 4.2: Closeup of Tier 1 sensor packets

version of Figure 4.1, giving a better look at each bit being sent across the network. The figures has been labeled to outline the location of each delay from Table 4.1, and also illustrates how the Tier 1 sensors wait for a synchronization pulse in order to begin sending data.

There is a difference between ideal and actual timing because the minimum ideal time does not factor in delays from the software running on top of actual hardware. Table 4.2 shows three different types of delays which cause the actual data transmission to be much slower. These delays depend on both how the software is written and the speed in which the processor operates at. In this thesis the PIC processor is set to operate at 32MHz.

Looking closer at Table 4.2 the delays shown represent the time it takes to enter the interrupt handler, send

| Description  | Symbol          | Min Ideal Time | Actual Time  |
|--|-----------------|----------------|--------------|
| Between STOP and START condition                         | $t_{buf}$       | $1.3\mu s$     | $19.40\mu s$ |
| Low period of the SCL clock                              | $t_{low}$       | $1.3\mu s$     | $1.26\mu s$  |
| High period of the SCL clock                             | $t_{high}$      | $0.6\mu s$     | $1.20\mu s$  |
| Set-up time for STOP condition                           | $t_{su;stop}$   | $0.6\mu s$     | $1.50\mu s$  |
| Between bytes of data                                    | $t_{byte\_buf}$ | $0.0\mu s$     | $19.70\mu s$ |
| Set-up time from START condition to beginning of address | $t_{su;addr}$   | $0.0\mu s$     | $19.80\mu s$ |
| Last data byte to start of STOP condition                | $t_{data;stop}$ | $0.0\mu s$     | $18.91\mu s$ |

Table 4.1: Minimum ideal and actual measured times for Tier 1 I<sup>2</sup>C communication

one byte of data by populating the SSPBUF register, and returning from the end of the interrupt handler. The first two delays together help dictate how much time  $t_{byte\_buf}$  takes. It is not until the SSPBUF register is filled that a byte of data can be transmitted across the I<sup>2</sup>C bus. Reducing either of these delays would improve the maximum throughput of data on the bus. The third delay, exiting from the interrupt handler, does not affect any of the timing values in Table 4.1, so attempting to reduce this delay would not make any improvement to data throughput. This only happens to be the case because it takes the I<sup>2</sup>C bus longer to transmit a byte of data,  $22.14\mu s$ , than it does to exit the interrupt handler. A way to shorten the actual timing needed to send data across the I<sup>2</sup>C bus would be to loop in the interrupt handler until all bytes from a packet are sent. Doing so would keep the software from having to delay  $11.63\mu s$  each byte just to enter the interrupt handler.

| Description   | Delay        |
|---|--------------|
| Entering interrupt handler                              | $11.63\mu s$ |
| From start of interrupt handler to sending byte of data | $3.88\mu s$  |
| Returning from interrupt handler                        | $12.00\mu s$ |

Table 4.2: Delays associated with the I<sup>2</sup>C software running on the 32MHz PIC processor

Once the ideal and actual timing values have been found, general equations can be derived to express how many sensors the on-body network can support for a given frequency. Equation 4.1a calculates the amount of time to send one byte of data along the network, represented by  $t_{byte}$ . This equation is then fed into equation 4.1b which calculates the amount of time it takes for any Tier 1 sensor to send a single packet of data. The variable  $bytes_{per\_packet}$  represents the number of bytes being sent by a packet of data. The third equation, 4.1c, expresses the number of sensors which can be supported once  $t_{packet}$  and the frequency of the Tier 1 sensors are known.

$$t_{byte} = 9 * (t_{high} + t_{low}) \quad (4.1a)$$

$$t_{packet} = ((t_{byte} + t_{byte\_buf}) * bytes_{per\_packet}) + t_{byte} + t_{data;stop} + t_{su;stop} + t_{su;addr} + t_{buf} \quad (4.1b)$$

$$num_{sensors} = 1 / (Frequency * t_{packet}) \quad (4.1c)$$

## 4.2.1 Current Setup

The number of bytes in a packet for the system described in this thesis alternates between 17 for full-updates and 11 for half-updates. With this piece of information known it is possible to sweep through various frequencies and give the accompanying amount of sensors supported. Only the full-updates are considered, since this represents the worst case scenario. Figure 4.3 compares the ideal I<sup>2</sup>C timing values to that of the actual values using equation 4.1c. Additionally, tests were performed by running the on-body network at specified frequencies to see how many sensors could be supported by the on-body network, represented by black squares in the figure. The tested and actual values will differ slightly since it is impossible to equip a fraction of a sensor to the network.

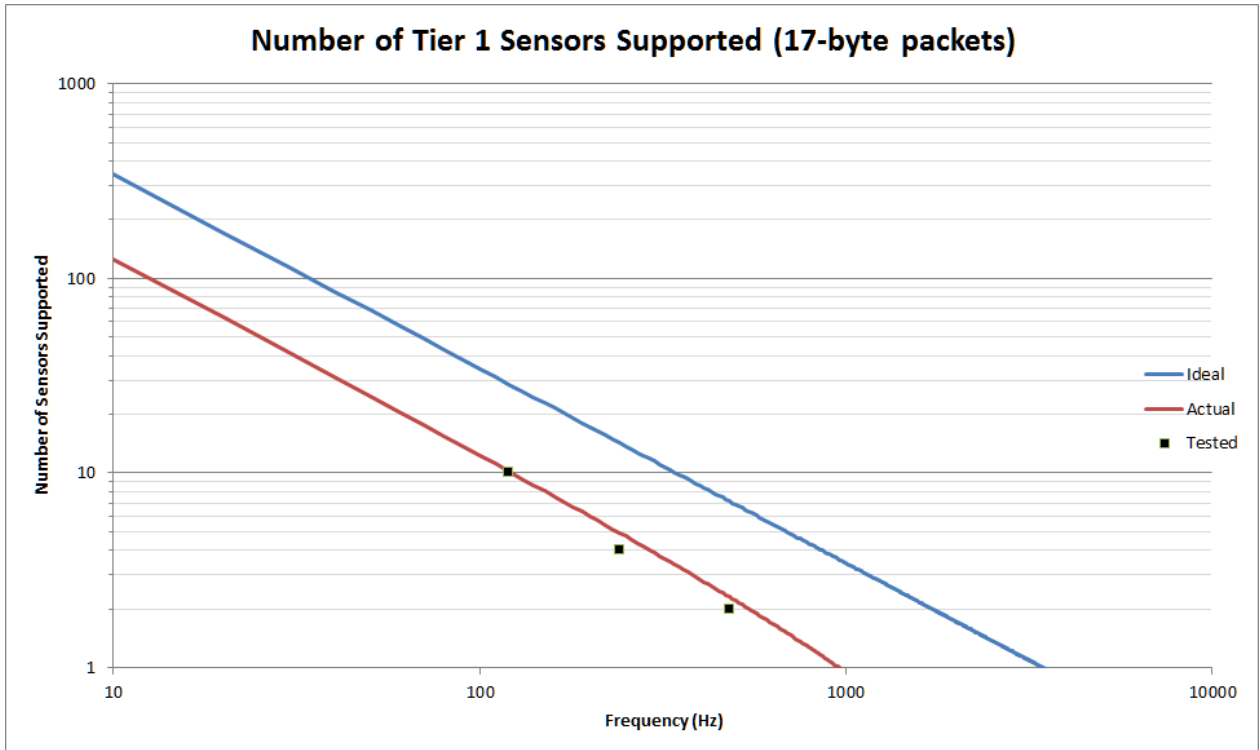


Figure 4.3: Frequency vs. sensors supported with 17-byte packets

## 4.2.2 Reducing Packet Size

It is possible to reduce the current packet size from 17 bytes down to 15 bytes, though not with the current hardware setup. Since the Tier 2 node converts data received from a Tier 1 sensor without needing any additional knowledge, it is possible to shift the computation done onto the Tier 1 sensors themselves. This would allow each Tier 1 sensor to calculate the quaternion for their respective limb before ever transmitting data on the on-body network. The packet would then be made up of one ID byte, eight quaternion bytes, and six accelerometer bytes. In order for this to be possible the current PIC processors found on a Tier 1 sensor would need to be upgraded enough to perform complex mathematic calculations quickly. Figure 4.4 shows the number of sensors gained based on frequency by reducing the packet size by two bytes. Only at lower frequencies does this difference in packet size make an impact. Minimal gain is seen once the Tier 1 sensors begin sampling at an adequate rate.

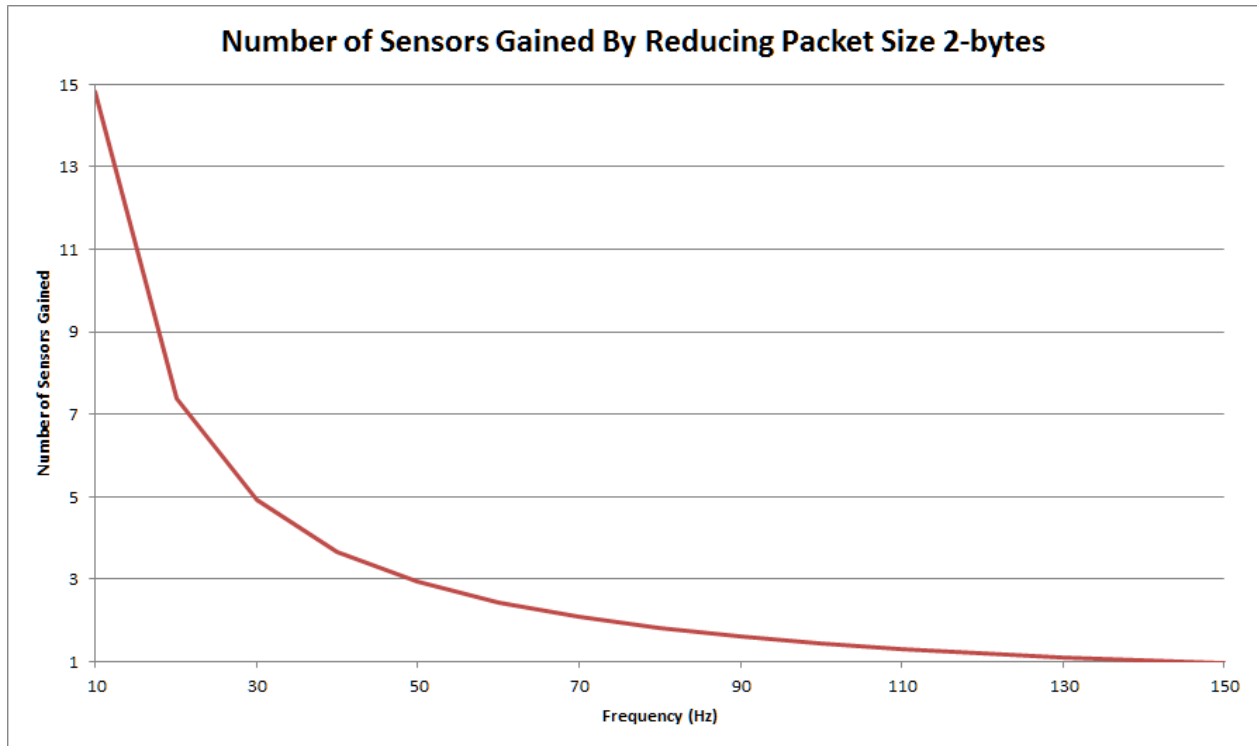


Figure 4.4: Frequency vs. sensors gained by reducing packet size 2 bytes

## 4.3 Off-body Communication

Off-body communication is defined as the communication of the Tier 2 node to a personal computer. Given the current hardware there are two possible ways to transfer the desired data, either through a wired or Bluetooth serial connection. Because both types of connections use serial to communicate, the software change to swap between the two becomes a simple matter of knowing which output stream to feed data into.

To help minimize the amount of data being sent per packet all bytes are concatenated together and have a dummy byte appended at the beginning and end so that the receiving application is able to decipher the individual packets. Each packet contains one byte identification, eight bytes for the quaternion, and two dummy bytes. The configuration is a 1-8-1 framing with no flow control.

$$max_{sensors} = pc_{baud} / (bytes_{sent} * (bits_{start} + bits_{data} + bits_{stop}) * frequency) \quad (4.2)$$

Equation 4.2 is the generalized equation to find out how many Tier 1 sensors can be supported when streaming data to a personal computer in real time. The 1-8-1 framing corresponds to  $bits_{start}$ ,  $bits_{data}$ , and  $bits_{stop}$  respectively.  $pc_{baud}$  is the baud rate in which the serial connection is transmitting at,  $bytes_{sent}$  is the number of bytes in a packet being sent by the Tier 2 node, and  $frequency$  is the rate the Tier 1 sensors are operating at.

### 4.3.1 Wired vs Bluetooth

The wired serial connection has a maximum baud rating of 230k, while Bluetooth has a maximum baud rating of 921k. Figure 4.5 gives a graphical representation of the two connections and the maximum number of sensors which can be supported for a specific frequency. Three tests were performed at the same frequency as those for the on-body communication. An application was run on the Tier 2 node to transmit simulated Tier 1 sensor information via the wired connection in order to establish how many sensors could actually be supported. These tests were not performed via Bluetooth because while the device is rated as being able to transmit at up to 921k, the Bluetooth receiver used in this thesis could not establish a connection at this baud rate.

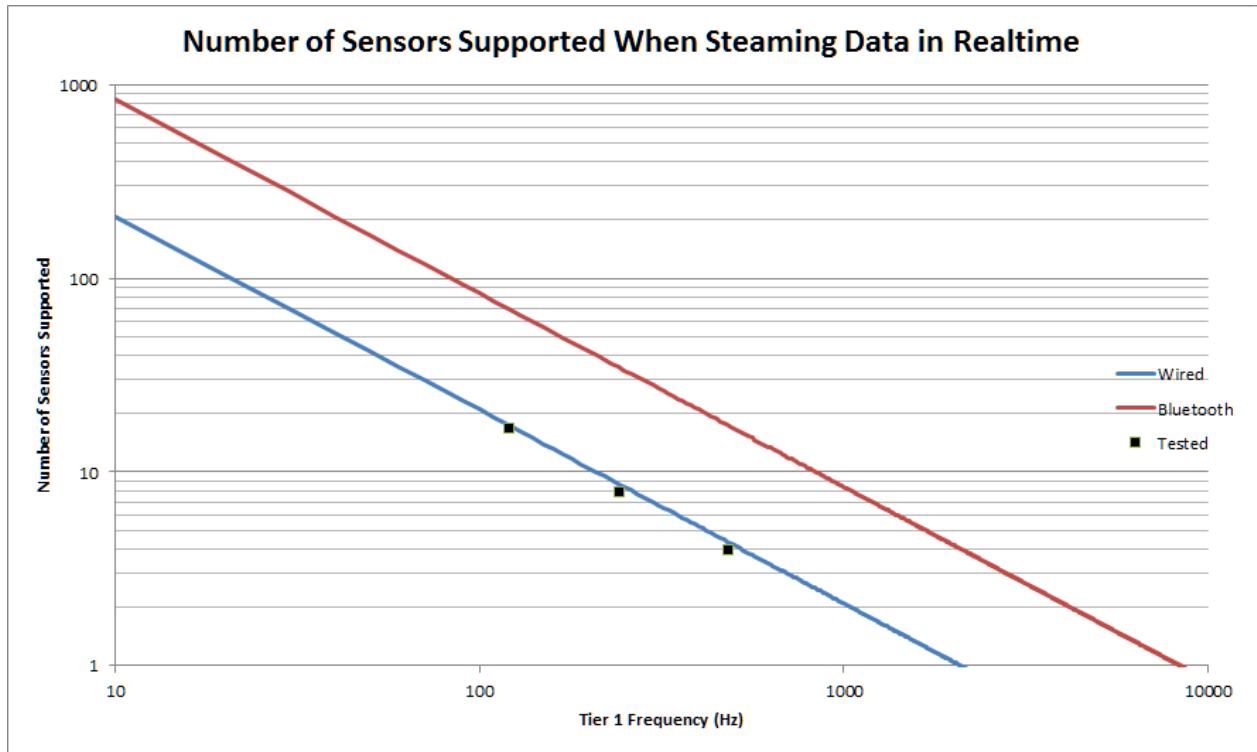


Figure 4.5: Frequency vs. sensors supported when streaming data in real time off-body

## 4.4 Potential Bottleneck

It is interesting to point out that the bottleneck in the current system resides with the on-body communication, even though I<sup>2</sup>C is operating faster than the wired serial. The reason for this is simply due to the amount of bytes, 17, that are being transferred per packet on-body, whereas only 11 bytes are being transferred off-body. If the bottleneck were a problem for the system described in this thesis the six bytes of data for the accelerometer could be removed, reducing the on-body packet size to 11 bytes.

# Chapter 5

## Results

This chapter summarizes the experiments performed to validate the accuracy of the self-contained garment. First, the set of tests used to determine the accuracy of the garment are explained in detail. Next, instructions explaining how the self-contained garment was tested and compared against a commercially available motion capture system are explained. The results of the overall comparison between the two systems are then explained. An analysis of why the two systems do not perfectly align is then explained while outlining the sources of error present. Finally, behavior of the self-contained garment is discussed with supporting data.

### 5.1 Motivation and Methodology

In order to test the accuracy of the self-contained garment it had to be compared directly with a system that was assumed to be accurate. A passive optical motion capture system, the *6 Pro-Reflex Optoelectronic System* by Qualisys, was chosen to compare against ours, since this system is commercially used and has been industry-tested for reliability [21]. This passive optical system is controlled through the Qualisys Track Manager software application, which records the optical marker movement and gives results with one to two millimeters of error [22]. To make the direct comparison six markers were attached to the self-contained garment at the shoulders, elbows, wrists, and the lower front chest, locations which are depicted in Figure 5.1. Tests would then be performed by capturing data from both systems at the same time. The passive optical capturing system was used to test not only the garment's ability to produce accurate results while stationary but also to test its ability to perform while in motion.

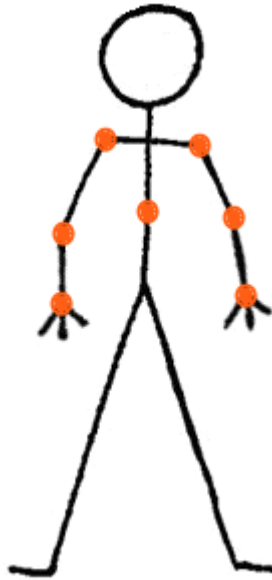


Figure 5.1: Placement of optical markers on body

A set of actions for users to perform also needed to be constructed. Specific actions were chosen to coincide with simple everyday tasks people might perform. These actions were kept concise and limited in number to make each test meaningful while encouraging redundancy to ensure consistency. Additional constraints existed due to the optical system being present. At the time of testing the optical system was limited in number of cameras and easily lost sight of the user outside of a certain area, forcing tests to be performed while stationary and facing only a percentage of the available room. As a result of these needs and limitations, eight tests were formed to test the upper body in a variety of poses. The eight tests have been summarized in Table 5.1 and are described in detail below.

The first test had the test subject stand up straight with their left arm in front of them and their right arm to their side, as illustrated in Figure 5.2. The second test swapped the actions of the left and right arms. These two tests placed the arms about 90 degrees apart from each other in order to sample the error seen when sensors were placed in a preferred position, horizontally, and in a non-preferred position, vertically.

The third and fourth tests start in the same position as the first two, except the user is instructed to bend the extended limb toward the torso. The test begins with the horizontal limb stretched with an angle around 180 degrees apart at the elbow; the user is then told to slowly bend their elbow until it reaches a 90 degree angle. The sweeping action's purpose is to test how accurately the limb's movement is recorded in comparison to the optical system. The user will perform these two actions again at the conclusion of the series of tests, labeled test seven and eight. This is done merely for checking consistency with the same subject.

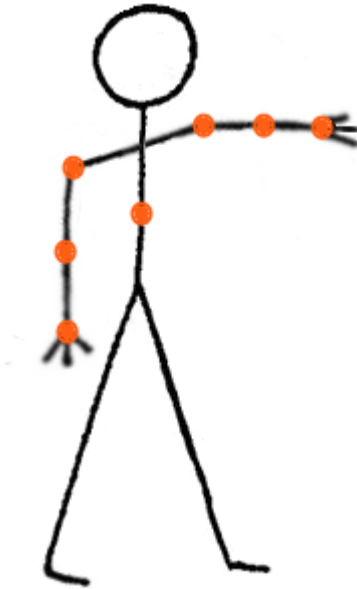


Figure 5.2: Left arm out including where the optical markers would be located on the garment

Test five has the user assume the *T-position* in which both arms are positioned ideally horizontal and parallel with the torso, illustrated in Figure 5.3. This test helps add to collected data for limbs that are placed at various horizontal positions.

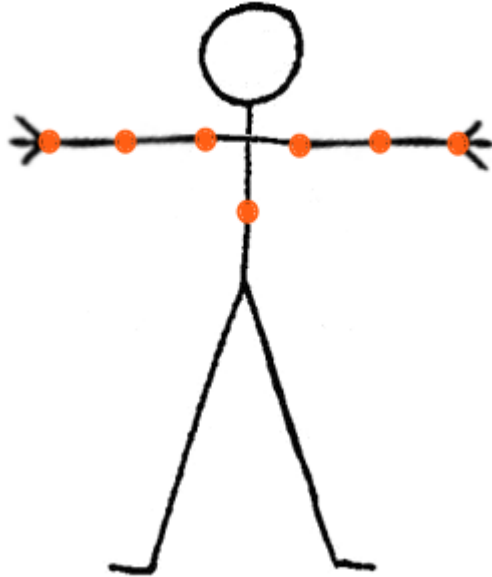


Figure 5.3: T-position including where the optical markers would be located on the garment

Test six has the subject sit properly in a wooden chair with their arms on the arm rest. It is important to note that the chair is wooden because it will not affect the digital compass readings negatively. This test differs from all of the others because of the arm rest being used. The arm rest causes the upper limbs to be positioned mostly vertically while the lower limbs are positioned mostly horizontally, thus testing the limbs at

different angles at the same time in a semi-controlled way.

| Test # | Description                  |
|--------|------------------------------|
| 1      | Left arm in front            |
| 2      | Right arm in front           |
| 3      | Left arm in front, bend 90°  |
| 4      | Right arm in front, bend 90° |
| 5      | T-position                   |
| 6      | Sitting in chair             |
| 7      | Left arm in front, bend 90°  |
| 8      | Right arm in front, bend 90° |

Table 5.1: Summary of the eight tests each user is instructed to perform

## 5.2 Comparing Motion Capture System Data

The two motion capture systems used record data in different ways. The garment uses a single Tier 1 sensor to produce a quaternion of the orientation of the body segment it is attached to, while the passive optical system uses two markers at the ends of a segment to track the absolute x, y, and z position of that segment. These two types of data are incompatible since a quaternion only describes rotation, not position. The goal here is to convert the quaternions acquired by the Tier 1 sensors and use that information to obtain the absolute x, y, and z positions of where our garment believes the optical balls would be located, allowing a direct comparison between both systems.

The two systems used have their own coordinate system. The optical motion capture system is able to define its own coordinate system, while the Tier 1 sensors use true north as the location of one of its axes, positive x in this thesis. In order to map one coordinate system into the other, a quaternion which represents the necessary rotation had to be created. This quaternion was made by placing a digital compass and two optical markers, one on either side, parallel with a ruler. The optical markers were spaced 51.45 cm apart from each other. Both systems recorded data while stationary. The quaternion given by the digital compass needed to be converted into vector form to compare against the optical system. This vector is created by multiplying the given quaternion by the digital compass' starting vector. For this thesis the digital compass' starting vector is in the positive x direction,  $[1\ 0\ 0]$ , because it is the point where heading, pitch, and roll are all equal to zero degrees. The cross and dot products between these two vectors were then taken to form the quaternion that maps the two coordinate systems correctly, as shown in Figure 5.4. Because of the one to two millimeter error present in the passive optical system, assuming no error from the digital compass, a worst-case error of about half a degree is present in any comparison between the two systems.

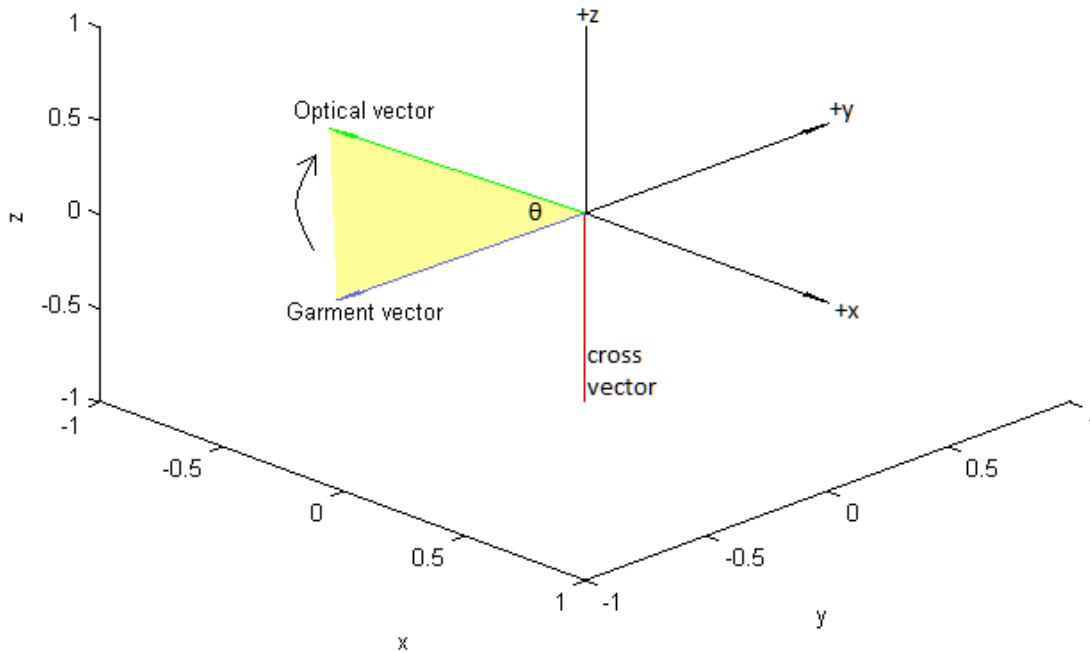


Figure 5.4: Finding the quaternion which maps the garment vector to the optical vector

### 5.2.1 Initial Body Structure Analysis

In order to compare the data between the two motion capture systems, several constants had to be defined. These constants were recorded using the first frame of data from both systems at the beginning of each test. Lengths of each limb segment were found by getting the difference between the optical markers at either end of each segment. The distance from the torso marker to each of the shoulders was also gathered to form a “triangle” representing the user’s rigid torso area. Figure 5.5 illustrates the six lengths that are recorded at the start of every test.

Vectors going from the torso to the left and right shoulders were created to keep track of the shoulder locations on the optical system, denoted as  $torso_{l_{opt}}$  and  $torso_{r_{opt}}$  respectively. The cross product of these two vectors produces a vector pointing in the direction the torso is facing, also known as the “forward vector” and shown in Equation 5.1. Additionally a vector going from the torso to the midpoint between the shoulders is also created, called the “up vector” and shown in Equation 5.2. The creation of these four vectors are illustrated in Figure 5.6. The two vectors, up and forward, describe the orientation of the optical motion capture system’s rigid torso. Likewise, the Tier 1 sensor attached to the garment’s torso can also be described with an up and forward vector. The up and forward vectors for the Tier 1 sensor are  $[1\ 0\ 0]$  and  $[0\ 0\ 1]$ , respectively in their default orientation, where heading, pitch, and roll are equal to zero.

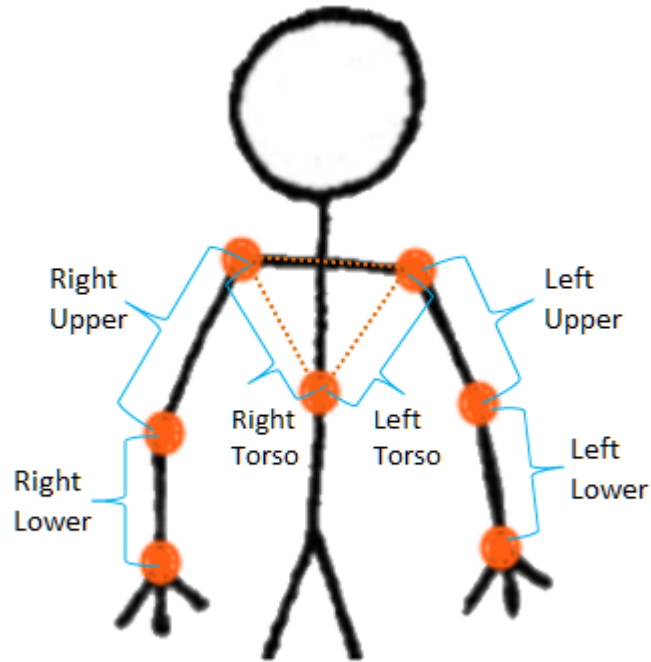


Figure 5.5: Location of the six segments whose length are initially taken

A quaternion that maps the torso of the optical motion capture system to the garment is called the offset quaternion. This quaternion is needed because the assumption made in this thesis is that both systems' torsos begin in the same orientation at the start of every test. The offset quaternion describes the initial difference between the two torsos. Equations 5.3a-d use the optical system's forward and up vectors to find a quaternion which describes its torso. The difference between the optical system's torso quaternion and garment's torso quaternion yields the desired offset quaternion. In the equation (scalar, vector) is used to denote a quaternion.

Finally the torso-to-shoulder vectors on the optical system need to be rotated. The offset quaternion is first applied to these vectors to map them into the orientation of the garment's torso. These vectors are then multiplied by the conjugate of the Tier 1 torso's quaternion from the garment. This second rotation maps the torso-to-shoulder vectors into the Tier 1's default orientation. Equations 5.4 and 5.5 show how these rotations are applied.

The newly found segment lengths, offset quaternion, and rotated torso-to-shoulder vectors are then used to construct the body model of the self-contained garment. Listing 5.1 gives the pseudo-code representation of how to determine these variables. The listing uses variables independant of those defined and used in the above mentioned equations.

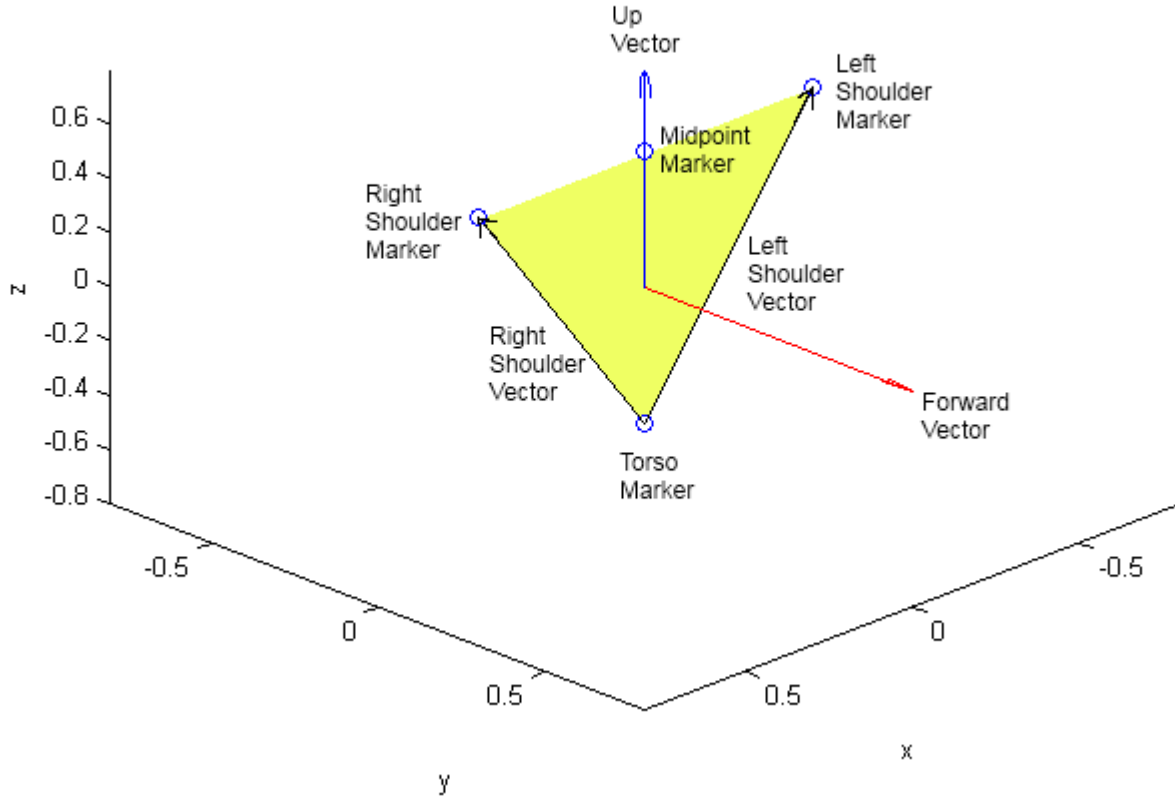


Figure 5.6: Finding the torso's orientation given three marker positions

$$\mathit{forward}_{opt} = \mathit{torsol}_{opt} \times \mathit{torsor}_{opt} \quad (5.1)$$

$$u\hat{p}_{opt} = \frac{(\mathit{lsmarker}_{opt} + \mathit{rsmarker}_{opt})/2 - \mathit{torsomarker}_{opt}}{\|(\mathit{lsmarker}_{opt} + \mathit{rsmarker}_{opt})/2 - \mathit{torsomarker}_{opt}\|} \quad (5.2)$$

$$\mathit{quatup} = (\arccos([1 \ 0 \ 0] \cdot u\hat{p}_{opt}), [1 \ 0 \ 0] \times u\hat{p}_{opt}) \quad (5.3a)$$

$$\hat{o}ut = \mathit{quatup} * [0 \ 0 \ 1] * \mathit{quatup}^{-1} \quad (5.3b)$$

$$\mathit{quatout} = (\arccos(\hat{o}ut \cdot \mathit{forward}_{opt}), \hat{o}ut \times \mathit{forward}_{opt}) \quad (5.3c)$$

$$\mathit{offsetquat} = (\mathit{quatup} * \mathit{quatout}) * \mathit{torsoquat}_{gar}^{-1} \quad (5.3d)$$

$$tor\hat{s}ol_{gar} = torsoquat_{gar}^{-1} * (offsetquat * tor\hat{s}ol_{opt} * offsetquat^{-1}) * torsoquat_{gar} \quad (5.4)$$

$$tor\hat{s}or_{gar} = torsoquat_{gar}^{-1} * (offsetquat * tor\hat{s}or_{opt} * offsetquat^{-1}) * torsoquat_{gar} \quad (5.5)$$

## 5.2.2 Data Mapping and Comparison

Having recorded the user's body structure using the first frame of data for a given test, the remaining frames are mapped out into a body model for comparison using the following steps. The offset quaternion previously found is applied to the garment's torso to correct for any differences in orientation that were seen at the start of the test, denoted  $torsofixedquat_{gar}$ . The garment's correct torso quaternion is then applied to the left and right torso-to-shoulder vectors found in the initial structure analysis. The resulting left and right torso-to-shoulder vectors are denoted  $torsofixed_{gar}$  and  $torsofixed_{gar}$  respectively and describe where the shoulders are located on the garment. Equations 5.6a-c show how to find these three variables. Finally, the Tier 1 sensors located on the upper and lower arms have their quaternions converted into vector form using the compass' starting vector mentioned previously. Equation 5.7 gives the general formula used to convert a Tier 1 quaternion into a vector. Once all of the sensors have been converted into unit vector form they are then multiplied by their respective segment length to be correctly sized.

The final step is to piece the vectors together and extract the absolute x, y, and z positions. In order to do this a single location on the optical motion capture system has to be assumed to be in the same location as the garment. For the comparisons made it is assumed that the lower torsos of both systems are located in the same place. The following steps focus on the left side of the body, but the same steps are performed to the right side. The left torso-to-shoulder's starting position is that of the lower torso, and the ending point is the garment's left shoulder location. The upper left arm's vector is then attached at the shoulder and ends at the elbow. Finally the lower arm is attached at the elbow and continues to the wrist. Absolute x, y, and z positions are known and comparisons between our garment and the optical system's markers can be directly made.

Listing 5.2 gives the pseudo-code representation of how to determine the garment's marker locations. The listing uses variables independent of those defined and used in the above mentioned equations. The steps taken in both this and the previous section together describe how to correctly compare the two garment's absolute x, y, and z position.

$$torsofixedquat_{gar} = offsetquat * torsoquat_{gar} \quad (5.6a)$$

$$torsol\hat{f}ixed_{gar} = torsoquatfixed_{gar} * tors\hat{o}l_{gar} * torsoquatfixed_{gar}^{-1} \quad (5.6b)$$

$$torsor\hat{f}ixed_{gar} = torsoquatfixed_{gar} * tors\hat{o}r_{gar} * torsoquatfixed_{gar}^{-1} \quad (5.6c)$$

$$out_{vec} = quat_{gar} * [1 \ 0 \ 0] * quat_{gar}^{-1} \quad (5.7)$$

Listing 5.1: Initial Body Structure function

```
function initialBodyStructure()
    for each segment
        get segment length
    end

    // tlso means torso left shoulder optical (system)
    tlso = torso-to-left-shoulder unit vector
    trso = torso-to-right-shoulder unit vector

    ms = calculate midpoint marker between tlso and trso

    // For the optical system
    forward_vector = tlso cross product trso
    up_vector = torso to ms unit vector

    // Calculate offset quaternion
    calculate quaternion A which maps [1 0 0] into up_vector
    rotate A by [0 0 1] and get resulting_vector
    calculate quaterion B which maps forward_vector into resulting_vector
    offset_quaterion = A * B * conj(garment_torso_quaternion)

    // tlsg means torso left shoulder garment
    // Calculate corrected torso-to-shoulder vectors for garment
    tlsg = (tlso * offset_quaterion) * garment_torso_quaternion
    trsg = (trso * offset_quaterion) * garment_torso_quaternion

    return forward_vector, up_vector, offset_quaternion, tlsg, trsg
end
```

Listing 5.2: Data Mapping and Comparison function

```
function dataMappingAndComparison()
// Correct garment's torso
corrected_garment_torso = offset_quaternion * garment_torso_quaternion

// Rotate garment's torso-to-shoulder vectors
rotated_tlsg = tlsg * corrected_garment_torso
rotated_trsg = trsg * corrected_garment_torso

// Convert garment quaternions into vectors
for each Tier 1 limb sensor
  multiply Tier 1 sensor quaternion by [1 0 0]
  store resulting vector
end

// Begin constructing garment body model
previous_loc = optical_torso_marker
// Each iteration determines a marker location on the left side of the garment
for vector = [rotated_tlsg, upper_left, lower_left]
  previous_loc = previous_loc + (vector * segment_length)
  save previous_loc
end

previous_loc = optical_torso_marker
// Each iteration determines a marker location on the right side of the garment
for vector = [rotated_trsg, upper_right, lower_right]
  previous_loc = previous_loc + (vector * segment_length)
  save previous_loc
end
// End constructing garment body model

return garment_marker_locations
end
```

---

### 5.3 Test Subject Results

Five test subjects, denoted SubjectA through SubjectE, were used to compare the data between our self-contained garment, with calibrated digital compasses, and the passive optical motion capture system. Each subject completed the eight specified tests described in Section 5.1 with each test lasting exactly twenty seconds. Twenty seconds was found to work well as it gave the subjects adequate time to perform all instructed tests. The pose and various angles of the body from both motion capture systems, shown in the following subsections, were then analyzed to show how accurate our self-contained garment performed compared to that of the optical motion capture system.

The raw data collected from these tests have been grouped together and are located in Appendix A. This data reflects the average error found, along with one standard deviation that our self-contained garment differed from the optical motion capture system. No filtering or error correction techniques have been applied to the data.

### 5.3.1 Overall Error Analysis

Figures 5.7 and 5.8 show the overall average and maximum errors seen between the two motion capture systems across all tests and subjects. These figures show absolute marker position error and body segment angle error. Tests that experienced error with optical marker movement were not included in these figures, as those tests were comparing against bad ground truth data. Section 5.3.2 explains this type of error in more detail.

Figure 5.7 shows how far off the garment is from the optical system at the six marker locations on the body. Error builds as the body model of the garment is constructed, so error in the markers will typically be greatest at the wrists. This figure shows that while the maximum average error seen across all eight tests is 135.1 mm at the wrist, the average mean at the same marker location is less than half. In addition to this, the error at the shoulders is relatively small because of the type of movements the user is instructed to perform in the eight tests. An assumption made when constructing the garment's body is that the torso is a rigid body and does not change in shape. If the user were instead instructed to, for example, dribble a basketball, the shape of the torso region would change and incur a much larger position error at the shoulder locations.

This figure also shows that the garment at each marker location has on average about 20 mm of error from that of the optical system. This puts the wrists at having about 60 mm of error when constructing the body model. The smart garment is going to be less accurate than the optical motion capture system. This is a trade-off that is made as a result of being a loose-fitting and self-contained system. The target audiences for this garment are those who do not need millimeter accuracy tracking but do need a system that can track motion in areas that conventional technology would not be feasible, e.g., monitoring daily movement in a home setting. The following sections go into detail and explain what approaches have been taken to minimize the error between the two systems.

Figure 5.8 shows the resulting angle errors for each segment of the garment compared to the optical motion capture system. These values show the range of error in which the Tier 1 sensors for a particular segment are, on average, misaligned with their optical system counterpart. Segment angle errors do not build up since they are not combined to form a body model. Since these errors do not build up, they are useful as supplement information to describe why the garment's overall pose does not match that of the optical system. Note that the error in torso means the angle in which the two motion capture systems differ by from the lower torso marker to the midpoint between the shoulders.

Segment angle errors combined with body segment lengths build the smart garment's body model, giving the

position errors seen in Figure 5.7. The marker positions for the upper body are repeatedly close to 20 mm off because the segments of the upper body are all about the same length. These errors would be different for the lower body due to it having different segment lengths in comparison. The garment had also been designed to fit subjects in the height range of 5'8" to 6'0" which constrains the range of upper body limb segment lengths. For subjects outside this height range, the average marker position error would be different.

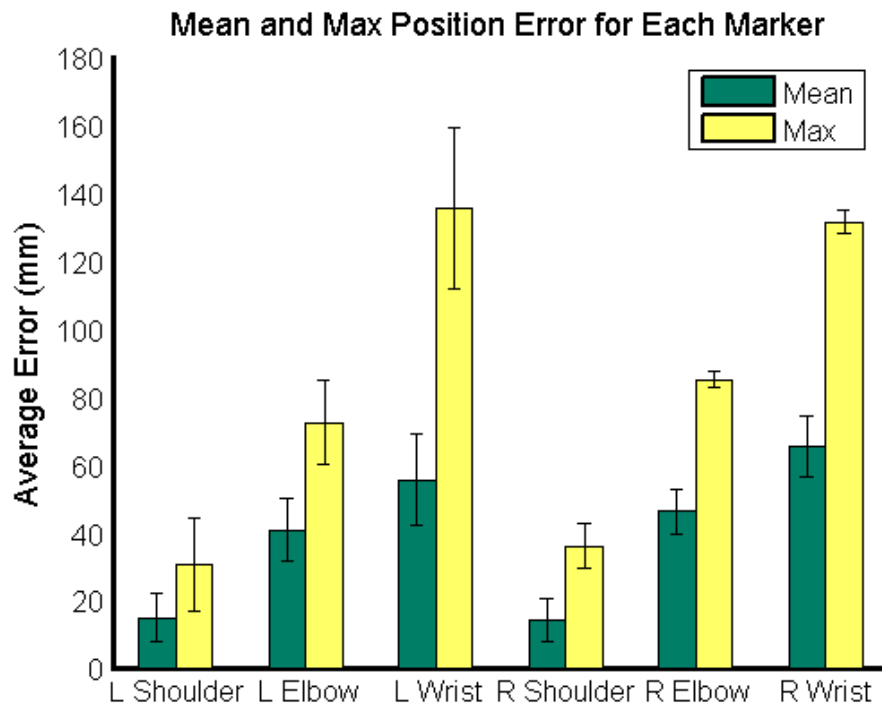


Figure 5.7: Mean and maximum average error and STD for marker positions across all test subjects and all tests

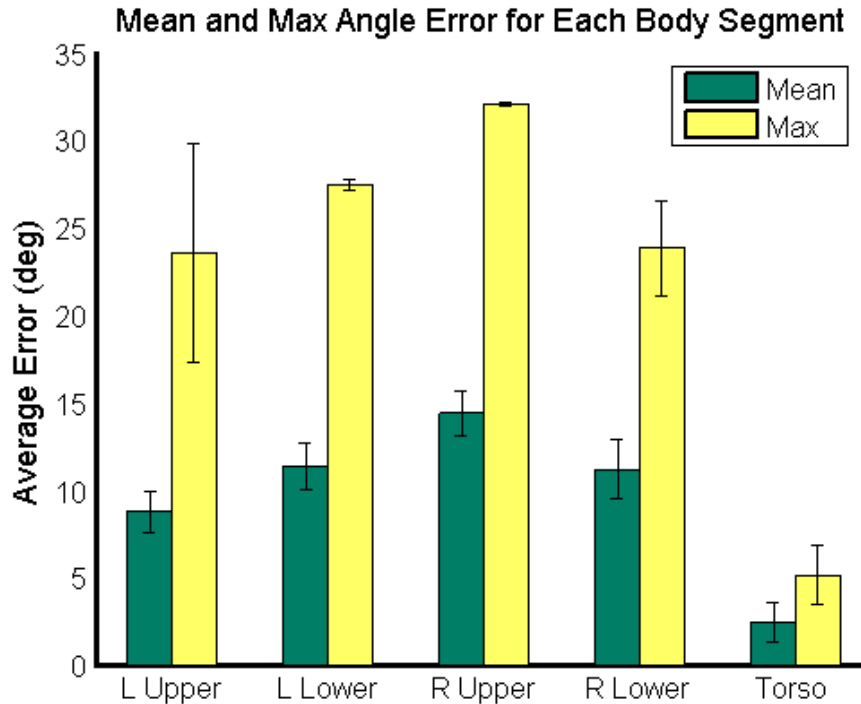


Figure 5.8: Mean and maximum average error and STD angles for segment angles across all test subjects and all tests. The torso error represents the angle which the systems differ by at the midpoint between the shoulders.

### 5.3.2 Sources of Error

There are two sources of error, hard-iron and loose fit of the garment, that contribute to the pose being off between the two systems. In addition, trouble recording accurate placement of the optical markers caused error in ground truth data. Steps have been taken to minimize and eliminate these types of error.

As mentioned at the beginning of this chapter, testing using the optical motion capture system proved to be rather difficult due to there being a limited number of available cameras to capture markers on the body. This forced the tests to be conducted while having the user face a specific direction in the room. Even with this constraint some tests had to be performed several times due to the optical system either having lost sight of a marker or having created extra markers due to reflection. Because the extra markers were being caused by reflections from the garment, they tended to act and move in a similar fashion that the actual markers did, proving difficult to sometimes eliminate. When processing the optical motion capture data using the Qualisys tracking manager application, jumps in marker locations were seen when only a few cameras had sight of a marker at a specific interval in time. Despite this, error caused by these jumps was minimal, with the largest occurring in SubjectE in Test #8, shown in Figure 5.9.

Figure 5.9 shows that SubjectE's garment shoulder locations differ by a large amount from that of the optical system. This error causes the elbow and wrist markers to also experience a large amount of error in their position. By looking at the optical system's raw torso x, y, and z position, shown in Figure 5.11, it is clear that a distinct jump in position occurred about one second into the test. This jump was caused by infrared reflections on the body causing the torso to appear in an incorrect location. This error caused the two motion capture systems to align incorrectly, as the offset quaternion used to align the two systems is calculated from the first frame of test data. By instead using the last frame to calculate the offset quaternion, a more accurate pose is created. Figure 5.10 shows the revised graph and how SubjectE's markers now match those of the other subjects.

The first source of error in the garment comes from its loose fit. Buckling in the clothing is possible due to the garment being made of thicker material, causing it to act more like a jacket than a t-shirt. When creating the sets of tests for each user to perform it was noticed that moving the upper arm inwards towards the torso region caused the cloth around the torso to be pushed, moving both the Tier 1 torso sensor and optical marker. This was taken into consideration when creating tests and as a result none of the tests performed in this thesis have a user press a segment of their body against another segment. These errors are a natural byproduct of the garment being a loose fitting item, and while the errors cannot be eliminated they can be minimized with the types of movements the user is asked to perform. Though in the general case there is no control over this type of error present in the garment.

The second source of error comes from hard-iron effects inside a building. All user tests performed had to be conducted in a specific room in order to test against the optical motion capture system. Section 5.3.3 shows several tests having been performed, highlighting the amount of heading error seen at each location. It is difficult to eliminate this error since the sensors are designed to operate correctly in a magnetically clean location; however, steps to reduce the error seen can and have been taken by calibrating each sensor prior to performing any comparison tests. Figure 5.12 shows one test which compares the elbow angle between both systems as the user bends it. Evidence of hard-iron error is present by comparing angles between the two systems. The garment's elbow angle is smaller than that of the optical systems' elbow at the beginning of the test by about  $10^\circ$ , but is greater at the end by about  $8^\circ$ . If no hard-iron error was present in the room, the error between the two systems would be relatively constant throughout the entire test. This conclusion is backed up by the fact that the range of error between the two systems seen through the full span of the test falls within the acceptable range found in Section 5.3.3.

A second way to tell that hard-iron error is present in the room is to look at the segment angle errors of each subject and test. Segments that are stationary exhibit a small standard deviation, while segments in

motion exhibit a much larger standard deviation. Figure 5.14 shows Test #4 which has the subject bend their right arm. The standard deviation is much larger in the right segments of the body than it is in the left segments of the body. In addition, the lower right segment has the highest average standard deviation because the subject was moving their lower right arm the most when bending. It is important to clarify that the larger standard deviation in error is seen when a sensor is in motion because the heading of that sensor is changing, and not simply due to the sensor exhibiting motion. Section 5.3.3 showed that error in heading changes based on the direction the sensor is facing in the room. To further illustrate this point, Figure 5.13 shows the difference in left wrist marker positions, over time, during a left arm bend. The left arm bend occurring is the same one shown in Figure 5.12. Distance error between markers remains relatively constant when no motion is occurring, and builds up when in motion.

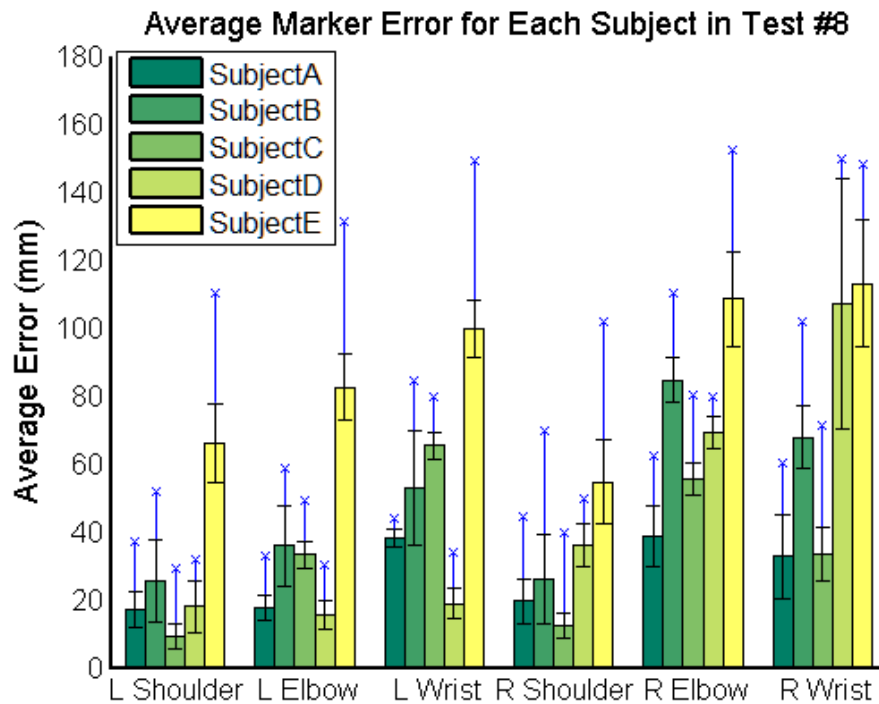


Figure 5.9: Average position error in Test #8, right arm bend, for all five subjects

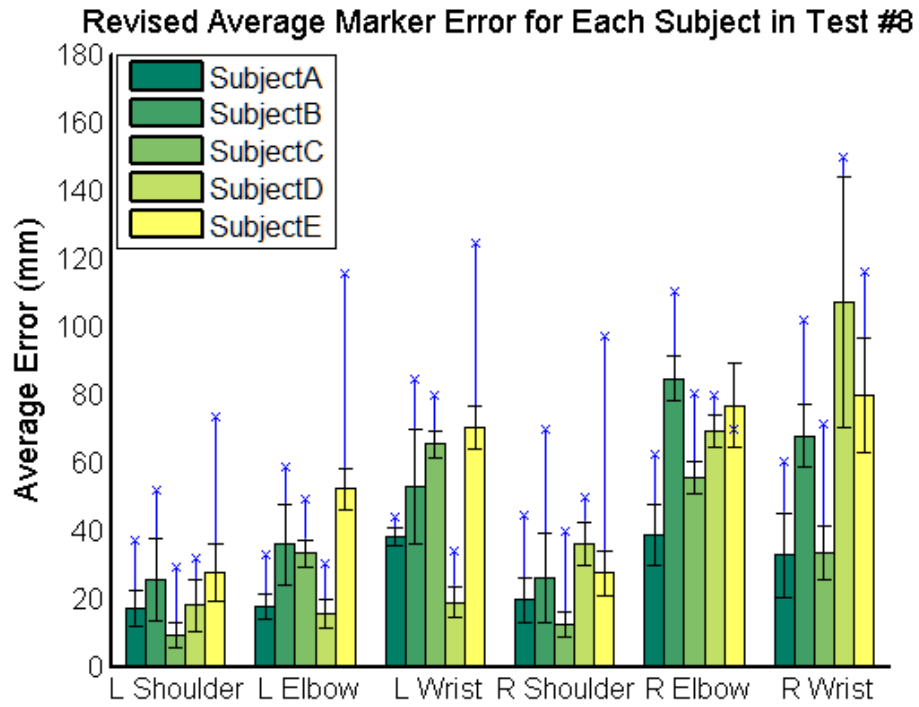


Figure 5.10: Average position error in Test #8, right arm bend, using subjectE's improved torso location

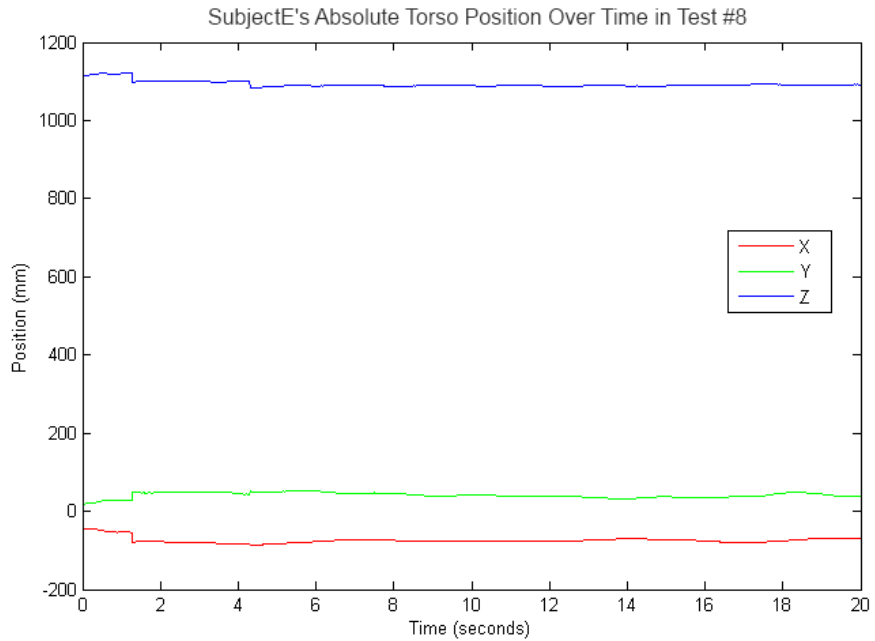


Figure 5.11: Absolute position of the torso over time for SubjectE in Test #8, right arm bend

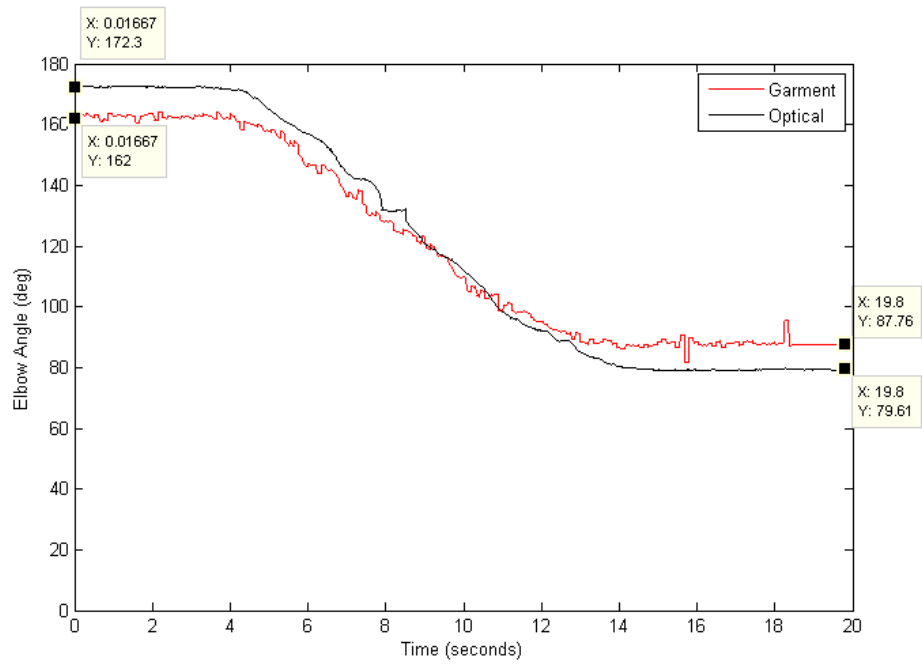


Figure 5.12: Left elbow bend highlighting hard-iron error

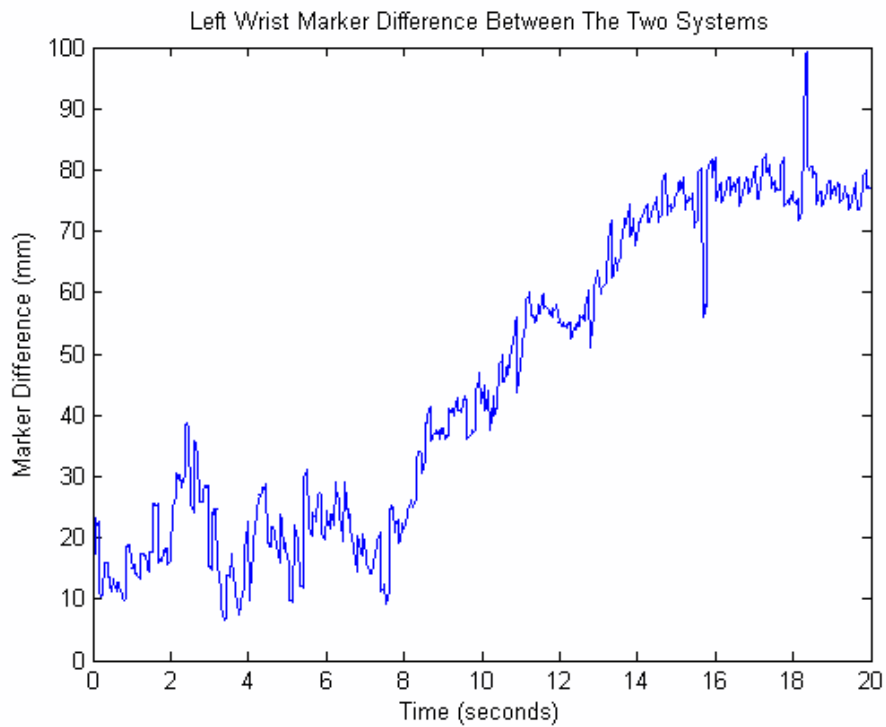


Figure 5.13: Difference in marker position between systems at the left wrist during a left arm bend

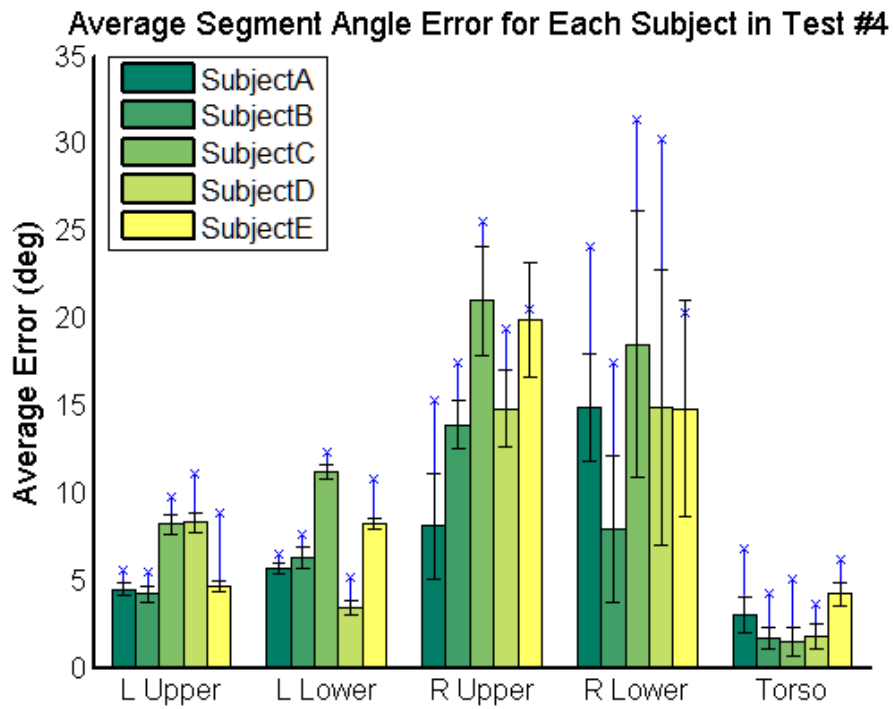


Figure 5.14: Average segment angle error in Test #4, right arm bend, for all five subjects. STD is larger in the right arm due to hard-iron error. The torso error represents the angle which the systems differ by at the midpoint between the shoulders.

### 5.3.3 Hard-iron Error

Before the performance of any test each digital compass was calibrated outdoors, as discussed in Section 3.3. To visualize the error in the magnetic field two sensors were placed on top of each other and attached to the center of a yard stick, as shown in Figure 5.15. These sensors had the same orientation with a gap in between to ensure one sensor would not adversely affect the other. The yard stick was rotated about the center, since magnetic field varies spatially. To make sure even measurements were taken this rotation was performed on top of a large protractor sketching.

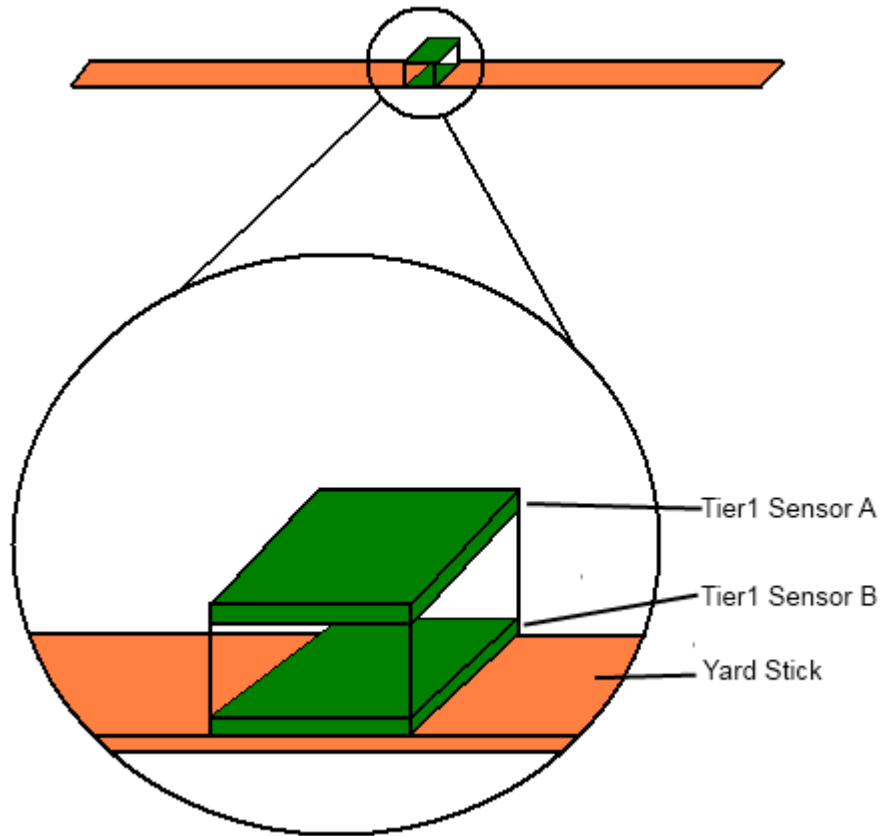


Figure 5.15: Attachment of sensors to a ruler for hard-iron error visualization

Results found that tests were consistent in the same location using the same sensor; however, different sensors gave different error graphs for the same location. Digital compasses other than the ones used in this thesis, such as those found in mobile phones, could not be used to tell where true north actually was since the areas tested in were not magnetically clean locations. As a result, graphs showing error in heading were created by finding a measured point where both digital compasses gave the same output for heading. This measured point is assumed to be correct and a “correct heading” is paired with each measured point by taking the difference of the corrected base heading and the measured rotation along the protractor. This results in the

digital compasses reporting the error seen at each measured heading. It is possible to do this because ideally hard-iron errors appear as a sine wave crossing the x-axis at  $0^\circ$  and  $180^\circ$ , so both sensors should cross the x-axis at the same location [17].

Figure 5.16 shows the error seen when rotating two digital compasses outdoors where it is magnetically clean. The y-axis shows the difference in heading of the digital compasses versus the ideal measurements. The x-axis shows the location from which the measurement was taken at on the protractor and does not reflect the degrees from true north. Table 5.2 shows the range of error for both sensors. This test shows that the digital compasses are only off by a few degrees, in their worst case, from true north. Also the calculated RMS error values for these compasses fall within the expected  $3^\circ$  RMS heading error mentioned in the sensor’s datasheet [15].

Figure 5.17 shows the same test performed inside of a building, referred to as Building A, with a similar magnetic field strength to that of the optical motion capture laboratory. The magnetic field’s strength was measured using a mobile phone application capable of reading its internal magnetometer sensor. Table 5.2 shows a drastic change in range of error, showing that material inside the building had affected the readings. To show that the error in the magnetic field can shift quickly a second test was performed within one foot of the previous test. Figure 5.18 shows the error from the second test, showing a range of error larger than that of the previous test for both sensors.

A fourth test was then performed in the same location where the motion capture suits would be compared. Figure 5.19 shows a  $7.5^\circ$  range of error in the first sensor and  $23^\circ$  range of error, the largest of the four tests, in the second sensor.

These four tests were done to demonstrate that large errors can occur in the digital compass sensors when used in locations that are not magnetically clean. This makes it difficult to predict exactly what error an individual compass will encounter. Prior to comparing the two motion capture systems, the digital compasses used in these experiments were taken outside and retested to make sure they had not become magnetized.

| Test # | Location                   | Compass A Error Range<br>deg | Compass B Error Range<br>deg |
|--------|----------------------------|------------------------------|------------------------------|
| 1      | Outside                    | 2.5                          | 4.8                          |
| 2      | Building A #1              | 4.5                          | 14.0                         |
| 3      | Building A #2              | 19.0                         | 15.0                         |
| 4      | Optical Motion Capture Lab | 23.0                         | 7.5                          |

Table 5.2: Maximum range of error between two compasses in various locations

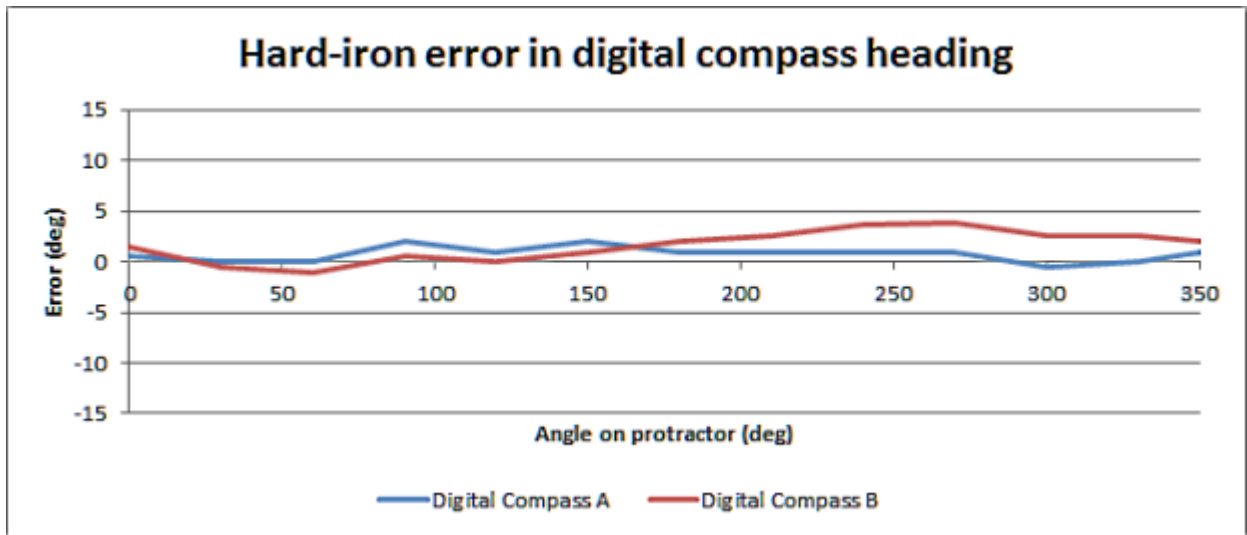


Figure 5.16: Hard-iron error of two compasses outdoors

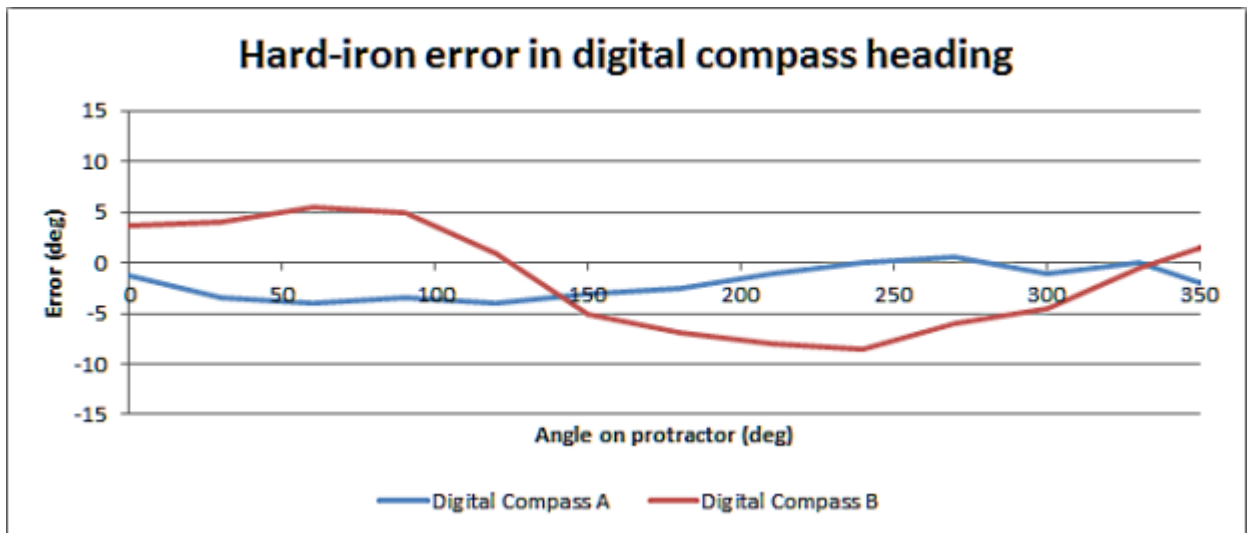


Figure 5.17: Hard-iron error of two compasses inside a building

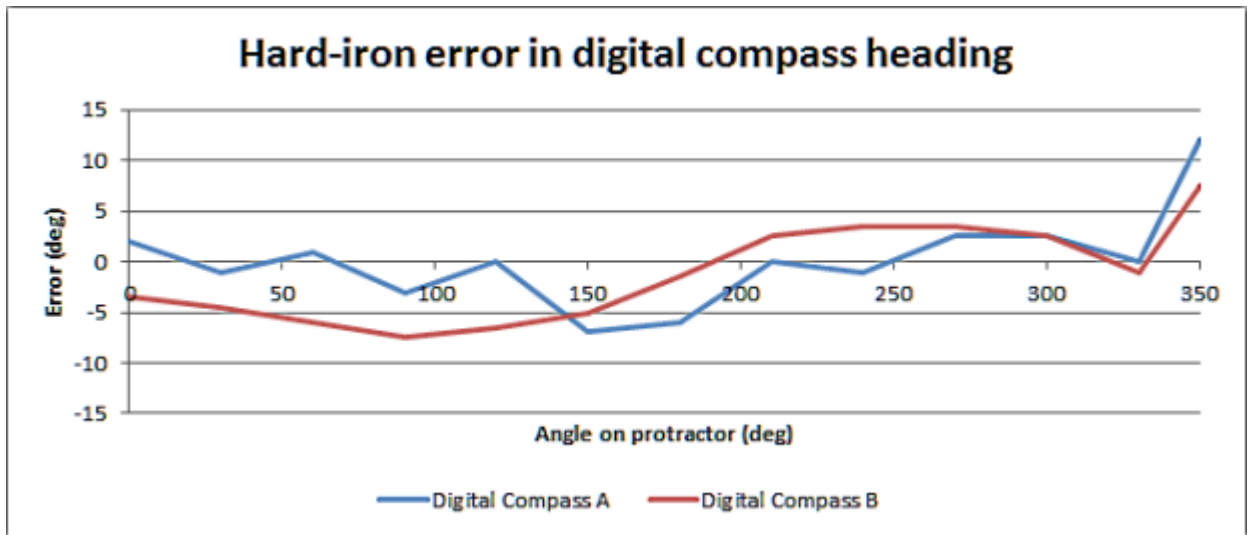


Figure 5.18: Hard-iron error of two compasses inside a building at a different location

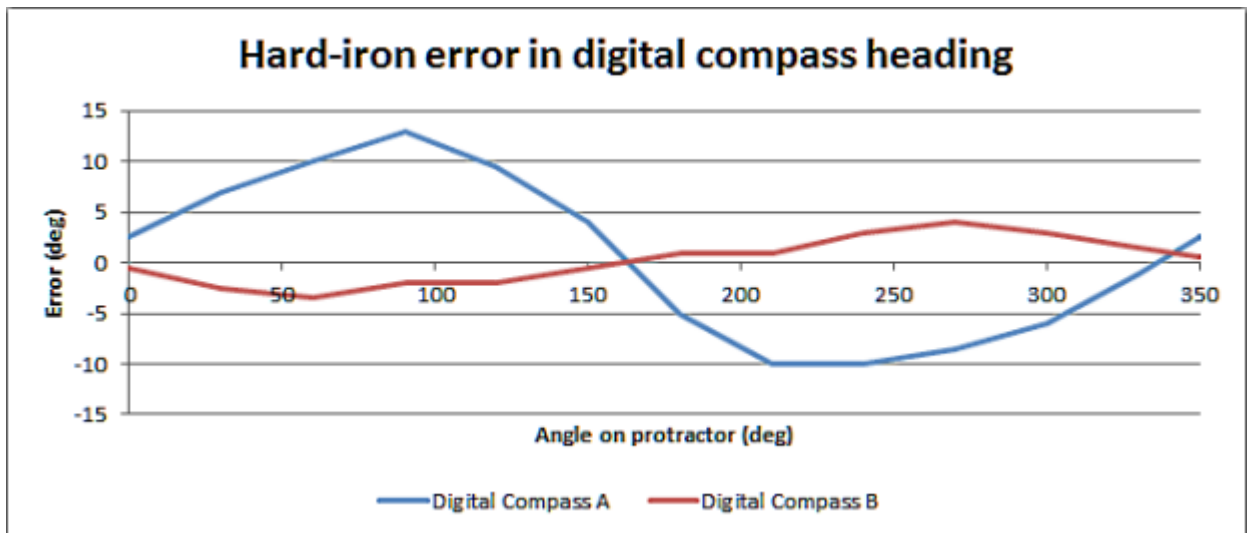


Figure 5.19: Hard-iron error of two compasses in subject testing room

### 5.3.4 Segment and Joint Angle Error

The segment and joint angle errors provide supplemental material to explain why error in the pose exists. Figures detailing average error for each test for both segment and joint angles were not provided, as neither exhibited any noticeable patterns between subjects or between tests. Instead, the average angle errors for every test have been taken to show the overall error seen during the study. These figures keep from grouping the five test subjects together in order to show that each subject performs similarly. Figure 5.20 shows the overall average angle error for each segment of the upper body. The torso error represents the angle that the upper part of the garment’s torso, where the shoulders are, differs from the optical system. Each segment’s angle error is relatively consistent between subjects as is its respective standard deviation. Furthermore, it is possible to reconstruct the marker error between systems by only knowing the angle error of the body segments and their respective segment lengths. Note that the hard-iron error observed in the testing laboratory, shown in Figure 5.19, has a range of  $23^\circ$  at a certain point in the room. The error seen in the segments are close to half this range. This amount of error is acceptable since the range of hard-iron error could be stronger at different points in the room, and because it is unreasonable to assume perfect sensor alignment on the garment at all time.

Similarly, Figure 5.21 shows the overall average joint angle error for each subject for all tests. The figure has six groups along the x-axis, three for each side of the body, which are needed to fully describe the four joints, two elbows and two shoulders, on the user’s upper body. Because the elbow is a hinged joint which is flexible in only one direction a single angle is capable of describing its full movement. Equation 5.8 shows how to calculate the angle, in degrees, that the garment and optical systems differ by. In this equation *upper* and *lower* represent the arm segments of the body. This angle is created by using the marker positions from both motion capture systems to generate vectors for the upper and lower arm segments. The dot product of the upper arm vector and lower arm vector for each system is then taken, and the difference between both systems generates the error for this joint.

$$\theta_{diff} = |\arccos(\mathit{upper}\hat{e}_{gar} \cdot \mathit{lower}\hat{e}_{gar}) - \arccos(\mathit{upper}\hat{e}_{opt} \cdot \mathit{lower}\hat{e}_{opt})| * \frac{180}{\pi} \quad (5.8)$$

The second joint, the shoulder, is unlike the elbow in that it is a ball-and-socket joint which allows for motion about a number of axes. For the experiments performed in this thesis, rolling about a limb is ignored since the loose fitting of the garment is, for the most part, unable to detect this type of movement. By ignoring detection of rolling of the shoulder from the equation, each shoulder is capable of being described using two

angles. The first angle is created by getting the component vector of the upper arm's vector parallel to the torso for both systems, as shown in Equations 5.9a-b. The dot product is then taken between these two component vectors to find the error along that plane, as shown in Equation 5.9e. The second angle performs a similar computation, but instead finds the component vector perpendicular to the torso, shown in Equations 5.9c-d with Equation 5.9f calculating the error perpendicular to the torso. These two angles describe the shoulder joint's error. In the below equations  $upper$  represents the upper arm's vector for the correct side of the body,  $fwd$  represents the vector perpendicular to the torso, and  $side$  represents the vector parallel to the torso for the correct side of the body. In the figures below,  $shoulder_{\parallel}$  reflects the angle parallel to the torso while  $shoulder_{\perp}$  reflects the angle perpendicular.

$$shldr_{\parallel gar} = upper_{gar} - (\arccos(upper_{gar} \cdot fwd_{gar}) * fwd_{gar}) \quad (5.9a)$$

$$shldr_{\parallel opt} = upper_{opt} - (\arccos(upper_{opt} \cdot fwd_{opt}) * fwd_{opt}) \quad (5.9b)$$

$$shldr_{\perp gar} = upper_{gar} - (\arccos(upper_{gar} \cdot side_{gar}) * side_{gar}) \quad (5.9c)$$

$$shldr_{\perp opt} = upper_{opt} - (\arccos(upper_{opt} \cdot side_{opt}) * side_{opt}) \quad (5.9d)$$

$$\theta_{\parallel} = \arccos(shldr_{\parallel gar} \cdot shldr_{\parallel opt}) * \frac{180}{\pi} \quad (5.9e)$$

$$\theta_{\perp} = \arccos(shldr_{\perp gar} \cdot shldr_{\perp opt}) * \frac{180}{\pi} \quad (5.9f)$$

The joint angle errors shown in Figure 5.21 show that a majority of the time the error is less than 10°. Furthermore, the average joint angle errors at the elbows have a smaller error than the segments which make up the joint due to hard-iron error affecting the sensors. This means that while the arms may not be aligned between systems, the error in those segments tend to be in the same direction causing the joints between systems to look similar.

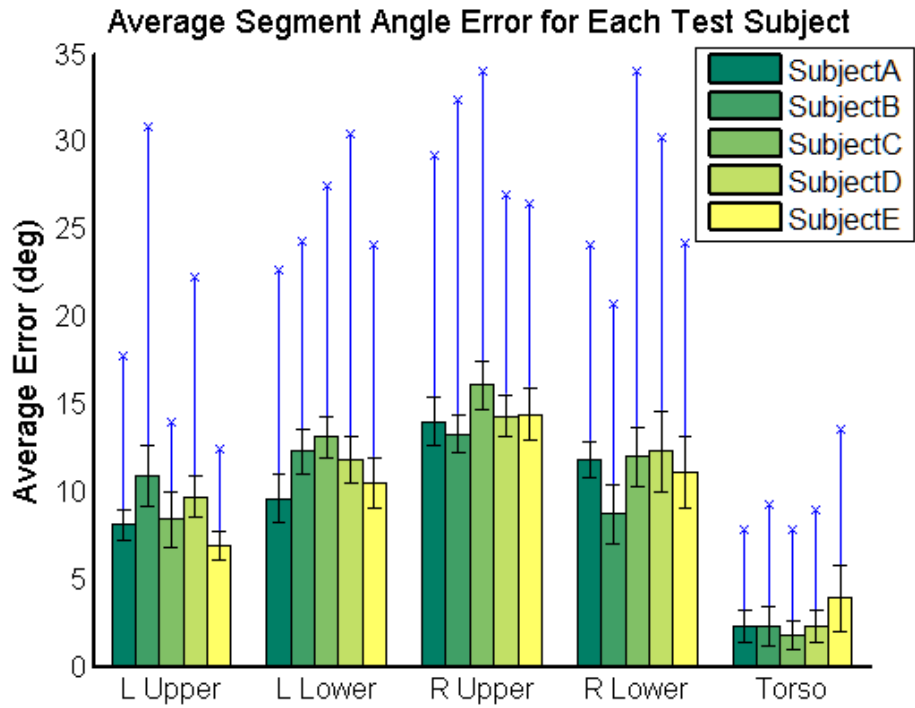


Figure 5.20: Average segment angle error for each test subjects across all tests. The torso error represents the angle which the systems differ by at the midpoint between the shoulders.

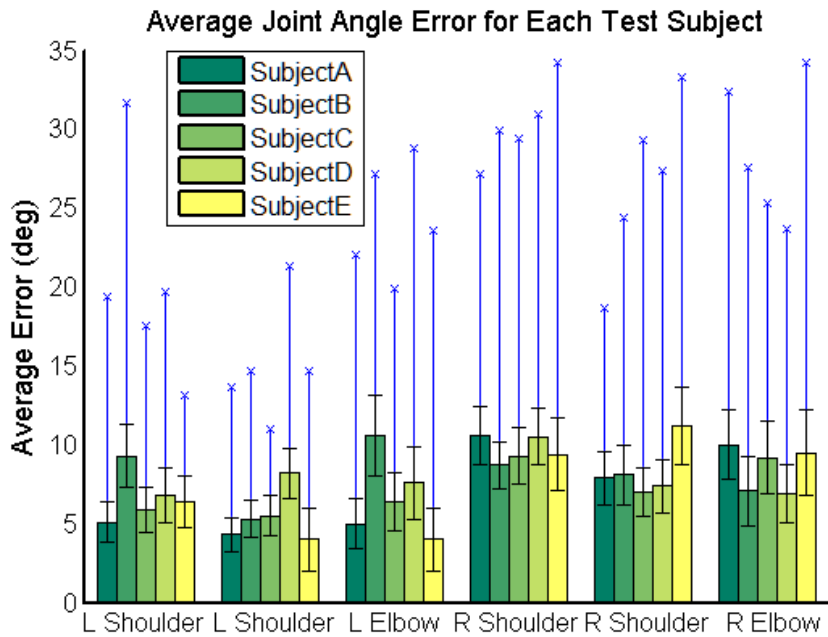


Figure 5.21: Average joint angle error for each test subjects across all tests

### 5.3.5 Analyzing Marker Position

Tables representing the marker position errors for all eight tests, across all five test subjects, are located in Appendix A. When the data in these tables are grouped together by test number they demonstrate behavior that can be easily observed in graph form. The figures in this section keep from grouping the five test subjects together in order to show that each subject performs similarly.

Error accumulates from torso to wrist as the body model is constructed. Each Tier 1 sensor on the garment gives its own orientation of that body segment, and is unaffected by neighboring sensors. When the body model of the garment is constructed, the lower torso is set to the same location as the optical system's lower torso. From there lengths of the body segments and Tier 1 sensor vectors are combined to identify where the other markers on the garment are. Listing 5.2 shows pseudo-code used to construct the garment markers. This error accumulates because the starting location of a segment is dependent on the ending location of its parent's segment. Figure 5.23 represents the summation of marker location error across all tests, for each test subject. The x-axis is grouped by marker location, going from shoulder to wrist. The upward curve in error as the body model is constructed is easily seen by viewing the graph from left to right.

A second behavior of this system is that body segments in motion exhibit a larger average error and standard deviation compare to those stationary. Section 5.3.2 has described this behavior in detail, showing how hard-iron error affects the digital compass as heading in the sensor changes.

A third behavior of this system is that the left and right sides of the body behave in an equal manner. This means error that affects the left side of the body also affects the right side of the body. Figure 5.23 is useful again to show this behavior. The eight tests performed, which are summarized in this figure, have the left and right sides of the body perform the same types of movements an equal number of times.

In addition to these behaviors shown across test data, outliers in particular body segments have also been observed. These anomalies occur due to sensor misalignment on the garment. An example of this is shown in Figure 5.22. SubjectA's right elbow and right wrist have a larger position error in them compared to the other four subjects performing the same test. By looking at the angle errors in the tables in Appendix A it is clear that this error is a result of the sensors having been misaligned on the garment. The right upper limb had an angle error of  $19.6^\circ$ , while the right lower limb had an angle error of  $17.9^\circ$ . Figure 5.24 shows the angle error of the upper and lower right limbs over time, to show that the error is constant and not caused by outlying data points.

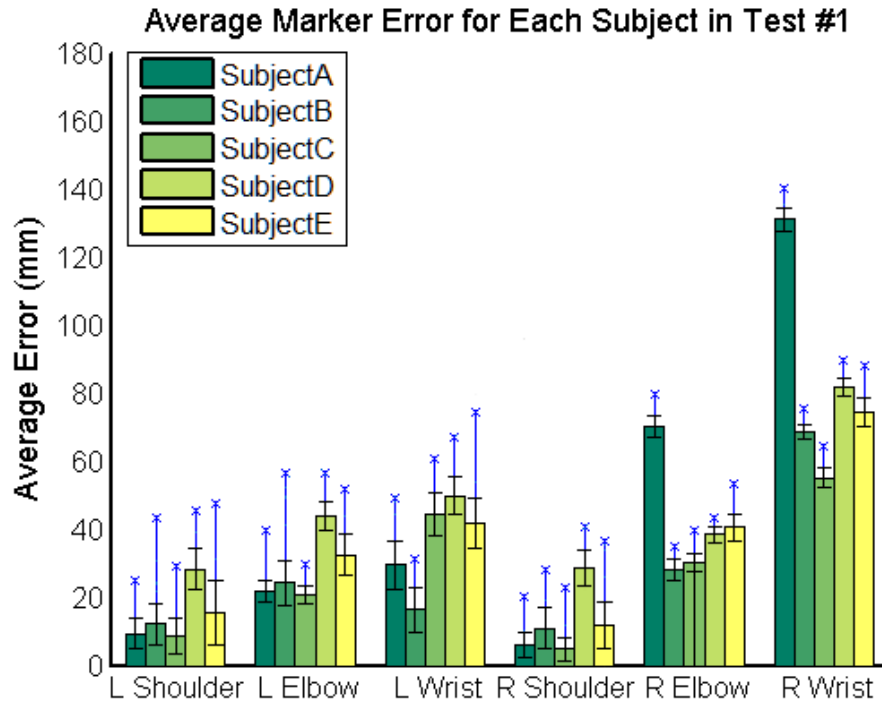


Figure 5.22: Average position error in Test #1, left arm out, for all five subjects

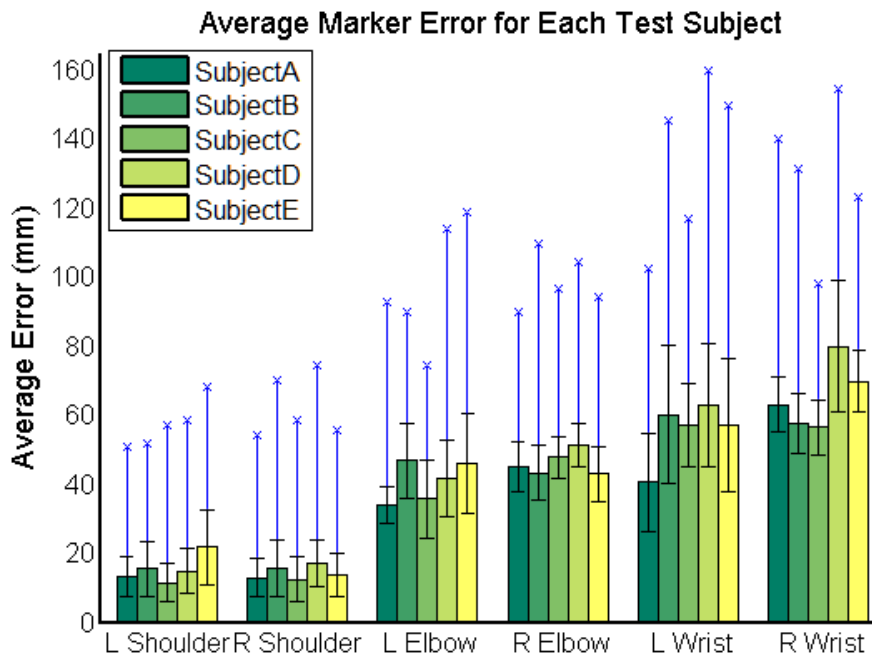


Figure 5.23: Average position error across all tests for each subject. Order of the x-axis has changed to highlight symmetry between the body

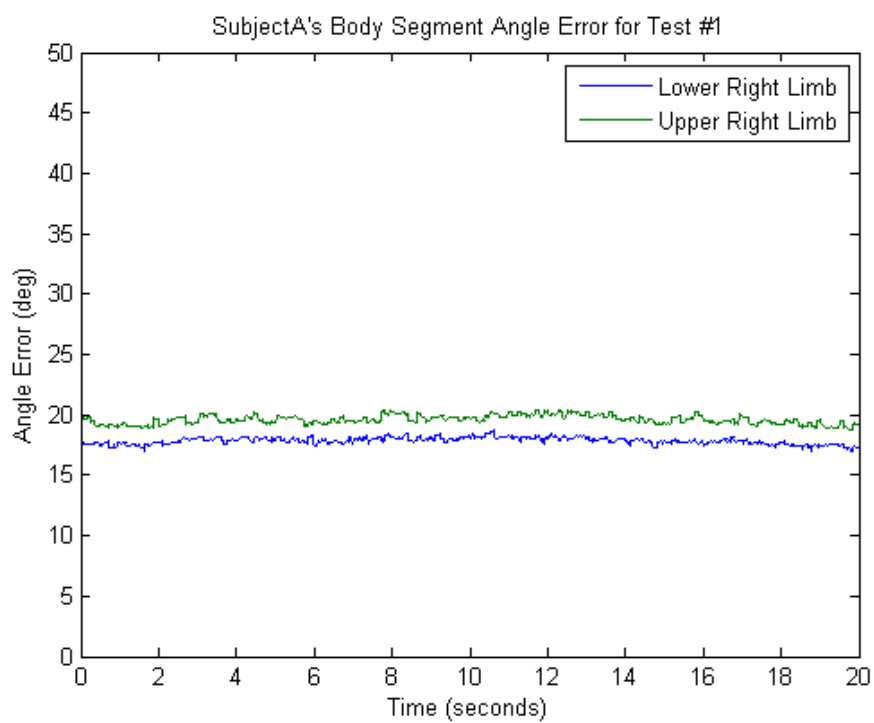


Figure 5.24: SubjectA's right side upper and lower limb error in Test #1, left arm out

## Chapter 6

# Conclusions and Future Work

### 6.1 Conclusion

The work performed in this thesis has characterized the sources of error that impact the smart garment's accuracy when compared to a commercial optical motion capture system. Doing so has defined the pros and cons associated with using a loose-fitting and self-contained garment to capture human motion. This work has also improved the framework previously designed at Virginia Tech's E-textiles Laboratory by correcting errors found in the design and using quaternions to easily track individual and overall pose of the body.

On average, the garment has been shown to have an error of 20 mm at the joint locations of the body when compared to the optical system. It is expected that the smart garment will be less precise in position tracking when compared to an optical system; however, the smart garment has other advantages which make up for it being slightly less accurate. Unlike the optical system, the smart garment is capable of directly measuring inertial movement of the body and is precise to 4 mg of acceleration [2]. The smart garment also provides a high mobility solution to capturing motion due to it being fully self-contained. Furthermore, the smart garment also appeals to those applications where a tight-fitting garment is not feasible, e.g., attaching a tight-fitting garment to patients in movement rehabilitation.

While the experiments conducted in this thesis were for the upper body only, the same techniques can be applied to the entire body. The sum of these experiments has shown that the smart garment is a viable alternative to current commercial motion capture systems for certain applications. The properties of the smart garment also help open up new paths for motion capture technology to be applied.

## 6.2 Future Work

One issue with the current design is the digital compasses being used. These sensors are designed to be used in devices that are operated outdoors, such as binoculars and laser range finders [15]. Section 3.3 shows how hard-iron error affects the current compass' readings. While it's not conclusive if a new set of compasses would fix or minimize this problem, it is something that should be looked into. The Xsens MVN Motion Capture suit is one successful commercial option also based on inertial measurements. This suit uses a different Honeywell compass, part of the HMC105X series, in its design [23]. The HMC105X series are specifically designed for applications such as Compassing and Magnetometry [24].

The data processed in this thesis has been raw data collected from the gyroscope and digital compass sensors. The Euler angles read by the digital compass relies on built in accelerometers, causing the output to give spikes of error while in motion. A better approach is to use the raw magnetometer readings from the digital compass which are unaffected by acceleration. These magnetometer values are then combined with readings from a dedicated accelerometer and gyroscope to produce a more accurate quaternion for the given Tier 1 sensor. A Kalman filter is traditionally used to combine these types of data together while minimizing noise seen from any one sensor [25].

# Bibliography

- [1] J. Edmison, “Hardware architectures for software security,” Master’s thesis, Bradley Department of Electrical and Computer Engineering, Virginia Tech, 2006.
- [2] J. Simmons, “A self-contained motion capture platform for e-textiles,” Master’s thesis, Bradley Department of Electrical and Computer Engineering, Virginia Tech, 2010.
- [3] P. Azad, A. Ude, T. Asfour, G. Cheng, and R. Dillmann, “Image-based markerless 3d human motion capture using multiple cues,” *International Workshop on Vision Based Human-Root Interaction*, 2006.
- [4] Z. Luo, I.-M. Chen, K. D. Nguyen, W. Ni, K. Li, C. Gu, C. K. Lim, and S. H. Yeo, “A wearable sensor network for the control of virtual characters,” *Advanced Intelligent Mechatronics*, pp. 1707–1712, July 2009.
- [5] M. Lapinski, “A wearable, wireless sensor system for sports medicine,” Master’s thesis, Massachusetts Institute of Technology, 2008.
- [6] Xsens. Xsens mvn–inertial motion capture. [Online]. Available: <http://www.xsens.com/en/general/mvn>
- [7] Vicon. Vicon mx motion capture system. [Online]. Available: <http://www.vicon.com/products/viconmx.html>
- [8] R. Guilemaud, Y. Caritu, D. David, F. Favre-Reguillon, D. Fontaine, and S. Bonnet, *Wearable eHealth Systems for Personalised Health Management: State of the Art and Future Challenges*. IOS Press, 2004, pp. 286–291.
- [9] D. Gafurov, K. Helkala, and T. Søndrol, “Biometric gait authentication using accelerometer sensor,” *Journal of Computers*, vol. 1, no. 7, pp. 51–59, November 2006.
- [10] S. Lovell, “A system for real-time gesture recognition and classification of coordinated motion,” Master’s thesis, Massachusetts Institute of Technology, 2005.

- [11] M. Quirk, "Inclusion of fabric properties in the design of electronic textiles," Master's thesis, Bradley Department of Electrical and Computer Engineering, Virginia Tech, 2009.
- [12] A. Love, "Automatically locating sensor position on an e-textile garment via pattern recognition," Master's thesis, Bradley Department of Electrical and Computer Engineering, Virginia Tech, 2009.
- [13] J. Chong, "Activity recognition processing in a self-contained wearable system," Master's thesis, Bradley Department of Electrical and Computer Engineering, Virginia Tech, 2008.
- [14] Sparkfun. LPR530AL Gyroscope Breakout Board. [Online]. Available: <http://www.sparkfun.com/products/9990>
- [15] Honeywell, "HMC6343 datasheet."
- [16] National Geophysical Data Center. Geomagnetism. [Online]. Available: <http://www.ngdc.noaa.gov/geomag/geomag.shtml>
- [17] R. Hubbard, *Boater's Bowditch*. International Marine/Ragged Mountain Press, 2000, pp. 43–45.
- [18] Tacktick Wireless Micro Compass. [Online]. Available: <http://www.tacktick.com/files/faq3.html>
- [19] H. Sun and P. Yang, "Design and research on errors compensation of digital compass," in *Mechatronics and Automation, 2009. ICMA 2009. International Conference on*. IEEE, 2009, pp. 4742–4747.
- [20] P. Semiconductors, "The I2C-Bus Specification: Version 2.1, January 2000." [Online]. Available: [http://www.nxp.com/acrobat\\_download2/literature/9398/39340011.pdf](http://www.nxp.com/acrobat_download2/literature/9398/39340011.pdf)
- [21] Qualisys. Motion Capture Systems. [Online]. Available: <http://www.qualisys.com/>
- [22] X. Zhang, personal communication, 2010.
- [23] Xsens MTi OEM. [Online]. Available: <http://www.xsens.com/en/general/mti-oem>
- [24] Honeywell, "HMC105x series datasheet."
- [25] C. Sul, S. Jung, and K. Wohn, "Synthesis of human motion using kalman filter."

# Appendix A

## Result Tables

| Test # | L Shoulder<br>mm | L Elbow<br>mm | L Wrist<br>mm | R Shoulder<br>mm | R Elbow<br>mm | R Wrist<br>mm |
|--------|------------------|---------------|---------------|------------------|---------------|---------------|
| 1      | 9.4 ± 4.6        | 22.1 ± 3.1    | 29.5 ± 7.0    | 6.2 ± 3.7        | 70.2 ± 3.2    | 131.1 ± 3.5   |
| 2      | 9.3 ± 5.0        | 28.4 ± 5.5    | 50.7 ± 3.9    | 8.9 ± 4.7        | 23.4 ± 8.4    | 35.7 ± 7.2    |
| 3      | 15.7 ± 8.2       | 38.5 ± 6.6    | 55.1 ± 29.0   | 13.4 ± 5.4       | 29.5 ± 5.3    | 42.1 ± 4.6    |
| 4      | 16.2 ± 5.4       | 20.8 ± 5.7    | 24.6 ± 7.6    | 21.7 ± 7.4       | 33.9 ± 13.1   | 52.9 ± 13.3   |
| 5      | 18.0 ± 7.6       | 55.3 ± 6.3    | 46.5 ± 6.5    | 14.2 ± 6.6       | 45.1 ± 5.5    | 57.5 ± 7.2    |
| 6      | 5.6 ± 2.5        | 53.6 ± 1.5    | 22.8 ± 2.4    | 3.8 ± 2.2        | 85.2 ± 1.9    | 87.8 ± 2.6    |
| 7      | 14.4 ± 7.0       | 35.1 ± 8.1    | 57.7 ± 24.9   | 16.0 ± 5.9       | 34.2 ± 5.9    | 64.6 ± 5.9    |
| 8      | 17.0 ± 5.3       | 17.7 ± 3.7    | 38.2 ± 2.8    | 19.5 ± 6.5       | 38.5 ± 9.0    | 32.7 ± 12.3   |

Table A.1: Mean and STD error of distance for each marker between suits for SubjectA

| Test # | L Shoulder<br>mm | L Elbow<br>mm | L Wrist<br>mm | R Shoulder<br>mm | R Elbow<br>mm | R Wrist<br>mm |
|--------|------------------|---------------|---------------|------------------|---------------|---------------|
| 1      | 12.2 ± 6.0       | 24.4 ± 6.6    | 16.4 ± 6.4    | 10.9 ± 6.1       | 28.1 ± 3.2    | 68.6 ± 2.1    |
| 2      | 16.7 ± 5.4       | 59.5 ± 7.0    | 77.6 ± 8.2    | 20.2 ± 7.1       | 13.8 ± 6.6    | 46.4 ± 10.5   |
| 3      | 27.3 ± 13.1      | 72.4 ± 12.4   | 68.5 ± 26.3   | 29.6 ± 12.6      | 21.0 ± 7.3    | 20.5 ± 7.4    |
| 4      | 11.2 ± 4.0       | 22.0 ± 4.7    | 23.8 ± 5.8    | 12.7 ± 4.1       | 51.6 ± 17.0   | 57.6 ± 15.7   |
| 5      | 9.0 ± 6.7        | 53.2 ± 5.1    | 44.3 ± 10.2   | 6.8 ± 5.7        | 29.2 ± 5.9    | 38.7 ± 5.5    |
| 6      | 5.0 ± 5.0        | 46.0 ± 3.3    | 99.8 ± 4.9    | 6.1 ± 4.7        | 85.0 ± 2.4    | 116.2 ± 2.6   |
| 7      | 17.1 ± 5.6       | 61.6 ± 22.4   | 98.4 ± 44.4   | 14.9 ± 7.1       | 33.2 ± 6.0    | 45.2 ± 6.2    |
| 8      | 25.7 ± 12.0      | 35.8 ± 11.8   | 52.9 ± 16.6   | 26.0 ± 13.0      | 84.5 ± 6.5    | 67.9 ± 9.1    |

Table A.2: Mean and STD error of distance for each marker between suits for SubjectB

| Test # | L Shoulder<br>mm | L Elbow<br>mm | L Wrist<br>mm | R Shoulder<br>mm | R Elbow<br>mm | R Wrist<br>mm |
|--------|------------------|---------------|---------------|------------------|---------------|---------------|
| 1      | 8.7 ± 5.4        | 20.8 ± 2.6    | 44.6 ± 6.3    | 4.9 ± 3.4        | 30.2 ± 2.7    | 55.1 ± 2.9    |
| 2      | 6.9 ± 4.0        | 48.3 ± 17.5   | 84.1 ± 16.8   | 12.8 ± 5.1       | 11.8 ± 5.9    | 55.1 ± 8.2    |
| 3      | 21.3 ± 6.6       | 36.0 ± 14.9   | 70.2 ± 19.6   | 26.9 ± 10.5      | 41.4 ± 9.9    | 61.3 ± 9.5    |
| 4      | 8.5 ± 3.7        | 30.1 ± 4.2    | 63.8 ± 4.3    | 9.0 ± 5.0        | 54.6 ± 9.3    | 39.6 ± 14.2   |
| 5      | 19.1 ± 10.1      | 42.9 ± 7.2    | 23.3 ± 8.8    | 18.4 ± 10.1      | 79.6 ± 5.7    | 73.7 ± 6.8    |
| 6      | 5.9 ± 3.3        | 37.4 ± 2.4    | 19.7 ± 3.9    | 5.1 ± 2.9        | 78.7 ± 2.9    | 86.8 ± 3.7    |
| 7      | 11.6 ± 5.1       | 38.9 ± 19.9   | 85.5 ± 17.9   | 10.4 ± 5.1       | 30.7 ± 2.7    | 47.7 ± 2.4    |
| 8      | 9.3 ± 3.5        | 33.2 ± 3.8    | 65.4 ± 4.0    | 12.3 ± 3.7       | 55.4 ± 4.7    | 33.5 ± 8.0    |

Table A.3: Mean and STD error of distance for each marker between suits for SubjectC

| Test # | L Shoulder<br>mm | L Elbow<br>mm | L Wrist<br>mm | R Shoulder<br>mm | R Elbow<br>mm | R Wrist<br>mm |
|--------|------------------|---------------|---------------|------------------|---------------|---------------|
| 1      | 28.4 ± 5.9       | 44.0 ± 4.3    | 50.0 ± 5.8    | 28.8 ± 5.2       | 38.5 ± 2.3    | 81.8 ± 2.5    |
| 2      | 12.1 ± 6.2       | 53.1 ± 8.6    | 55.6 ± 8.7    | 8.9 ± 4.2        | 39.8 ± 4.0    | 47.8 ± 6.3    |
| 3      | 8.7 ± 4.2        | 41.6 ± 11.5   | 85.4 ± 16.3   | 9.2 ± 5.1        | 23.7 ± 5.0    | 78.1 ± 4.9    |
| 4      | 8.7 ± 4.5        | 36.7 ± 8.8    | 48.3 ± 9.2    | 13.5 ± 5.4       | 57.3 ± 6.3    | 104.1 ± 34.9  |
| 5      | 24.5 ± 10.6      | 34.8 ± 12.0   | 48.1 ± 12.8   | 19.6 ± 9.9       | 68.2 ± 12.1   | 66.0 ± 15.0   |
| 6      | 3.9 ± 3.2        | 40.2 ± 1.6    | 60.8 ± 2.9    | 4.3 ± 3.1        | 79.5 ± 2.8    | 85.6 ± 3.4    |
| 7      | 14.1 ± 6.6       | 67.9 ± 22.1   | 135.1 ± 43.4  | 17.8 ± 10.9      | 35.1 ± 8.4    | 69.5 ± 9.0    |
| 8      | 18.1 ± 7.6       | 15.7 ± 4.3    | 18.8 ± 4.6    | 36.2 ± 6.4       | 69.1 ± 4.8    | 107.3 ± 36.8  |

Table A.4: Mean and STD error of distance for each marker between suits for SubjectD

| Test # | L Shoulder<br>mm | L Elbow<br>mm | L Wrist<br>mm | R Shoulder<br>mm | R Elbow<br>mm | R Wrist<br>mm |
|--------|------------------|---------------|---------------|------------------|---------------|---------------|
| 1      | 15.7 ± 9.5       | 32.6 ± 6.0    | 41.9 ± 7.3    | 11.8 ± 7.0       | 40.7 ± 4.0    | 74.5 ± 4.3    |
| 2      | 21.3 ± 6.7       | 37.8 ± 9.5    | 46.6 ± 10.4   | 12.5 ± 4.0       | 33.9 ± 11.3   | 82.2 ± 10.3   |
| 3      | 30.8 ± 13.8      | 71.9 ± 32.4   | 99.5 ± 50.2   | 12.1 ± 3.1       | 49.7 ± 4.9    | 60.6 ± 6.5    |
| 4      | 28.9 ± 22.7      | 38.6 ± 16.5   | 59.4 ± 10.5   | 24.5 ± 16.1      | 47.6 ± 20.2   | 70.8 ± 23.9   |
| 5      | 24.0 ± 9.3       | 39.9 ± 10.7   | 34.5 ± 7.6    | 14.2 ± 6.1       | 32.5 ± 7.1    | 80.8 ± 9.0    |
| 6      | 12.9 ± 4.3       | 44.4 ± 3.8    | 22.7 ± 5.6    | 14.0 ± 2.8       | 60.9 ± 3.7    | 70.7 ± 4.7    |
| 7      | 19.3 ± 10.0      | 56.8 ± 22.7   | 95.5 ± 42.6   | 7.9 ± 4.3        | 36.6 ± 4.4    | 48.9 ± 4.5    |
| 8      | 66.0 ± 11.6      | 82.6 ± 9.8    | 99.9 ± 8.4    | 54.7 ± 12.6      | 108.4 ± 13.9  | 113.0 ± 18.6  |

Table A.5: Mean and STD error of distance for each marker between suits for SubjectE

| Test # | L Upper deg | L Lower deg | R Upper deg | R Lower deg | Torso deg |
|--------|-------------|-------------|-------------|-------------|-----------|
| 1      | 5.5 ± 0.7   | 11.2 ± 1.0  | 19.6 ± 0.4  | 17.9 ± 0.3  | 1.3 ± 0.7 |
| 2      | 7.9 ± 0.4   | 8.7 ± 0.4   | 6.6 ± 2.9   | 16.0 ± 0.8  | 1.7 ± 0.9 |
| 3      | 6.6 ± 2.5   | 11.5 ± 3.8  | 12.1 ± 0.3  | 4.8 ± 0.3   | 2.9 ± 1.3 |
| 4      | 4.5 ± 0.4   | 5.7 ± 0.3   | 8.1 ± 3.0   | 14.9 ± 3.1  | 3.0 ± 1.0 |
| 5      | 14.4 ± 1.3  | 3.7 ± 1.1   | 12.7 ± 1.2  | 8.2 ± 1.3   | 2.4 ± 1.0 |
| 6      | 16.6 ± 0.1  | 15.2 ± 0.3  | 28.2 ± 0.5  | 7.4 ± 0.4   | 1.1 ± 0.5 |
| 7      | 6.1 ± 1.1   | 11.8 ± 3.6  | 14.1 ± 0.6  | 10.3 ± 0.4  | 2.6 ± 1.1 |
| 8      | 3.0 ± 0.3   | 8.8 ± 0.4   | 10.4 ± 2.5  | 14.8 ± 1.6  | 3.1 ± 1.1 |

Table A.6: Mean and STD angle error at each segment of the body for SubjectA

| Test # | L Upper deg | L Lower deg | R Upper deg | R Lower deg | Torso deg |
|--------|-------------|-------------|-------------|-------------|-----------|
| 1      | 5.0 ± 0.7   | 9.6 ± 0.8   | 7.4 ± 0.4   | 13.2 ± 0.6  | 1.9 ± 0.9 |
| 2      | 10.4 ± 0.7  | 6.0 ± 0.6   | 5.3 ± 2.3   | 12.4 ± 0.8  | 3.2 ± 1.0 |
| 3      | 23.5 ± 6.2  | 13.5 ± 2.8  | 4.7 ± 1.2   | 1.8 ± 0.6   | 2.6 ± 1.0 |
| 4      | 4.2 ± 0.5   | 6.3 ± 0.6   | 13.9 ± 1.4  | 7.9 ± 4.2   | 1.7 ± 0.6 |
| 5      | 14.8 ± 1.2  | 15.8 ± 1.0  | 10.2 ± 1.5  | 7.8 ± 0.9   | 1.1 ± 0.9 |
| 6      | 13.2 ± 0.1  | 19.6 ± 1.1  | 32.0 ± 0.1  | 11.3 ± 0.4  | 0.9 ± 0.9 |
| 7      | 13.3 ± 3.5  | 16.9 ± 2.3  | 6.4 ± 0.5   | 3.9 ± 0.5   | 3.1 ± 1.2 |
| 8      | 3.2 ± 0.4   | 10.7 ± 1.4  | 26.2 ± 1.3  | 11.3 ± 5.6  | 3.9 ± 2.0 |

Table A.7: Mean and STD angle error at each segment of the body for SubjectB

| Test # | L Upper deg | L Lower deg | R Upper deg | R Lower deg | Torso deg |
|--------|-------------|-------------|-------------|-------------|-----------|
| 1      | 6.8 ± 0.4   | 13.2 ± 0.8  | 8.7 ± 0.3   | 7.4 ± 0.3   | 1.4 ± 0.8 |
| 2      | 11.3 ± 5.6  | 11.4 ± 0.3  | 6.3 ± 1.7   | 15.3 ± 1.0  | 1.5 ± 0.6 |
| 3      | 4.3 ± 1.2   | 12.6 ± 3.8  | 9.4 ± 0.8   | 6.9 ± 0.4   | 3.0 ± 0.9 |
| 4      | 8.2 ± 0.6   | 11.2 ± 0.4  | 21.0 ± 3.1  | 18.5 ± 7.6  | 1.5 ± 0.8 |
| 5      | 9.5 ± 0.9   | 10.5 ± 0.9  | 24.9 ± 0.9  | 7.0 ± 0.6   | 2.6 ± 1.4 |
| 6      | 12.8 ± 0.2  | 17.3 ± 0.3  | 28.0 ± 0.9  | 11.3 ± 0.3  | 1.0 ± 0.5 |
| 7      | 8.0 ± 3.1   | 18.3 ± 3.1  | 9.3 ± 0.5   | 5.4 ± 0.4   | 1.3 ± 0.7 |
| 8      | 6.0 ± 0.6   | 10.4 ± 0.3  | 20.9 ± 3.2  | 23.8 ± 2.7  | 1.8 ± 0.6 |

Table A.8: Mean and STD angle error at each segment of the body for SubjectC

| Test # | L Upper deg | L Lower deg | R Upper deg | R Lower deg | Torso deg |
|--------|-------------|-------------|-------------|-------------|-----------|
| 1      | 8.9 ± 0.5   | 12.1 ± 1.0  | 9.3 ± 0.4   | 15.0 ± 0.3  | 4.3 ± 0.8 |
| 2      | 9.7 ± 0.4   | 0.8 ± 0.3   | 12.4 ± 1.1  | 11.9 ± 1.1  | 1.8 ± 1.0 |
| 3      | 10.7 ± 1.1  | 18.4 ± 3.5  | 8.6 ± 0.3   | 17.1 ± 0.3  | 1.2 ± 0.8 |
| 4      | 8.3 ± 0.6   | 3.4 ± 0.4   | 14.8 ± 2.2  | 14.9 ± 7.9  | 1.8 ± 0.7 |
| 5      | 5.4 ± 1.7   | 7.0 ± 1.1   | 20.0 ± 2.1  | 2.6 ± 1.5   | 3.3 ± 1.4 |
| 6      | 12.9 ± 0.1  | 27.4 ± 0.3  | 25.4 ± 0.4  | 8.3 ± 0.5   | 0.8 ± 0.5 |
| 7      | 16.5 ± 5.1  | 23.8 ± 3.6  | 9.3 ± 1.3   | 11.1 ± 0.7  | 2.3 ± 1.2 |
| 8      | 5.3 ± 0.4   | 1.2 ± 0.3   | 14.5 ± 2.2  | 17.3 ± 6.5  | 3.1 ± 0.7 |

Table A.9: Mean and STD angle error at each segment of the body for SubjectD

| Test # | L Upper deg | L Lower deg | R Upper deg | R Lower deg | Torso deg  |
|--------|-------------|-------------|-------------|-------------|------------|
| 1      | 8.7 ± 0.7   | 13.8 ± 1.1  | 13.0 ± 0.4  | 10.6 ± 0.4  | 2.3 ± 1.3  |
| 2      | 4.5 ± 0.9   | 3.2 ± 0.9   | 9.9 ± 2.3   | 23.0 ± 1.9  | 3.7 ± 1.4  |
| 3      | 5.3 ± 1.7   | 11.6 ± 2.8  | 12.1 ± 0.6  | 3.3 ± 0.7   | 3.0 ± 1.5  |
| 4      | 4.7 ± 0.3   | 8.2 ± 0.3   | 19.9 ± 3.3  | 14.8 ± 6.2  | 5.2 ± 4.7  |
| 5      | 5.9 ± 1.2   | 7.2 ± 1.0   | 9.0 ± 1.2   | 14.4 ± 1.0  | 3.0 ± 1.2  |
| 6      | 11.5 ± 0.1  | 17.9 ± 0.9  | 19.7 ± 0.4  | 10.3 ± 0.3  | 2.0 ± 1.2  |
| 7      | 6.4 ± 1.4   | 16.0 ± 3.8  | 11.7 ± 1.0  | 4.0 ± 0.8   | 2.2 ± 1.4  |
| 8      | 8.1 ± 0.5   | 6.0 ± 0.7   | 20.1 ± 3.1  | 8.4 ± 4.3   | 10.1 ± 2.6 |

Table A.10: Mean and STD angle error at each segment of the body for SubjectE

| Test # | L Shoulder 1 deg | L Shoulder 2 deg | L Elbow deg | R Shoulder 1 deg | R Shoulder 2 deg | R Elbow 2 deg |
|--------|------------------|------------------|-------------|------------------|------------------|---------------|
| 1      | 4.1 ± 0.9        | 0.9 ± 0.6        | 1.1 ± 0.8   | 16.8 ± 1.0       | 11.7 ± 1.0       | 1.6 ± 0.7     |
| 2      | 1.5 ± 0.7        | 6.7 ± 1.1        | 7.2 ± 0.6   | 6.8 ± 2.8        | 4.8 ± 2.3        | 21.0 ± 3.1    |
| 3      | 6.5 ± 2.0        | 2.0 ± 1.3        | 11.1 ± 5.4  | 5.9 ± 1.0        | 8.2 ± 1.4        | 4.1 ± 0.8     |
| 4      | 2.3 ± 2.1        | 3.3 ± 1.5        | 5.3 ± 0.5   | 7.3 ± 4.1        | 3.1 ± 2.3        | 17.2 ± 4.1    |
| 5      | 4.9 ± 2.1        | 11.1 ± 1.5       | 3.4 ± 0.9   | 1.9 ± 1.5        | 12.9 ± 1.4       | 6.5 ± 2.3     |
| 6      | 15.5 ± 0.4       | 6.7 ± 0.5        | 0.6 ± 0.5   | 26.0 ± 0.5       | 9.6 ± 1.2        | 4.8 ± 1.1     |
| 7      | 5.0 ± 1.6        | 2.0 ± 1.4        | 9.5 ± 3.3   | 8.9 ± 1.2        | 9.6 ± 1.6        | 3.2 ± 1.3     |
| 8      | 1.0 ± 0.7        | 1.7 ± 1.0        | 1.9 ± 0.5   | 11.6 ± 2.8       | 3.6 ± 2.0        | 21.4 ± 4.0    |

Table A.11: Mean and STD angle error at each joint of the body for SubjectA

| Test # | L Shoulder 1 deg | L Shoulder 2 deg | L Elbow deg | R Shoulder 1 deg | R Shoulder 2 deg | R Elbow 2 deg |
|--------|------------------|------------------|-------------|------------------|------------------|---------------|
| 1      | 5.2 ± 1.1        | 3.1 ± 0.7        | 13.2 ± 1.1  | 2.0 ± 1.0        | 6.6 ± 1.2        | 3.3 ± 1.0     |
| 2      | 5.1 ± 0.9        | 12.2 ± 1.0       | 3.9 ± 0.7   | 3.0 ± 2.2        | 3.6 ± 2.4        | 7.4 ± 2.6     |
| 3      | 21.8 ± 6.4       | 4.0 ± 2.6        | 10.7 ± 8.3  | 1.1 ± 0.8        | 3.4 ± 1.4        | 5.4 ± 1.5     |
| 4      | 5.3 ± 0.8        | 1.0 ± 0.6        | 5.3 ± 0.5   | 2.5 ± 2.1        | 7.5 ± 3.7        | 8.0 ± 5.7     |
| 5      | 14.2 ± 1.3       | 9.0 ± 1.2        | 20.4 ± 1.8  | 10.5 ± 1.8       | 7.7 ± 0.9        | 2.4 ± 1.1     |
| 6      | 7.8 ± 1.0        | 10.0 ± 0.6       | 8.7 ± 0.7   | 25.6 ± 1.1       | 18.0 ± 0.7       | 12.3 ± 0.7    |
| 7      | 8.7 ± 2.4        | 2.8 ± 2.1        | 17.2 ± 6.4  | 8.5 ± 1.5        | 0.9 ± 0.5        | 1.9 ± 0.8     |
| 8      | 6.2 ± 2.2        | 0.5 ± 0.4        | 5.9 ± 1.5   | 16.0 ± 1.7       | 17.3 ± 4.1       | 16.3 ± 4.3    |

Table A.12: Mean and STD angle error at each joint of the body for SubjectB

| Test # | L Shoulder 1 deg | L Shoulder 2 deg | L Elbow deg | R Shoulder 1 deg | R Shoulder 2 deg | R Elbow 2 deg |
|--------|------------------|------------------|-------------|------------------|------------------|---------------|
| 1      | 2.7 ± 0.9        | 4.5 ± 0.8        | 10.0 ± 0.9  | 7.4 ± 0.9        | 3.3 ± 0.9        | 0.5 ± 0.5     |
| 2      | 7.6 ± 1.0        | 10.6 ± 1.7       | 4.6 ± 5.2   | 2.5 ± 1.8        | 5.9 ± 2.2        | 14.6 ± 2.8    |
| 3      | 2.5 ± 1.5        | 6.2 ± 2.4        | 6.5 ± 3.5   | 4.7 ± 1.3        | 4.6 ± 0.6        | 2.9 ± 1.1     |
| 4      | 3.6 ± 0.7        | 6.7 ± 0.9        | 4.6 ± 0.5   | 8.3 ± 3.2        | 7.1 ± 2.9        | 14.7 ± 4.4    |
| 5      | 7.2 ± 2.1        | 1.0 ± 0.7        | 18.1 ± 0.5  | 2.4 ± 1.7        | 25.3 ± 1.4       | 11.0 ± 1.5    |
| 6      | 12.6 ± 0.7       | 4.2 ± 0.9        | 0.3 ± 0.3   | 27.1 ± 0.9       | 5.8 ± 1.6        | 2.7 ± 1.5     |
| 7      | 4.9 ± 3.6        | 6.4 ± 2.2        | 4.6 ± 2.7   | 9.0 ± 0.9        | 0.9 ± 0.7        | 4.1 ± 0.9     |
| 8      | 6.0 ± 0.8        | 4.6 ± 0.8        | 2.8 ± 0.7   | 12.8 ± 4.0       | 2.9 ± 2.1        | 22.8 ± 5.5    |

Table A.13: Mean and STD angle error at each joint of the body for SubjectC

| Test # | L Shoulder 1<br>deg | L Shoulder 2<br>deg | L Elbow<br>deg | R Shoulder 1<br>deg | R Shoulder 2<br>deg | R Elbow 2<br>deg |
|--------|---------------------|---------------------|----------------|---------------------|---------------------|------------------|
| 1      | 12.2 ± 1.2          | 6.4 ± 1.0           | 6.8 ± 0.6      | 4.8 ± 1.1           | 5.4 ± 0.7           | 0.6 ± 0.5        |
| 2      | 3.3 ± 0.8           | 10.5 ± 1.1          | 3.4 ± 0.5      | 8.6 ± 2.3           | 7.1 ± 1.9           | 11.4 ± 2.6       |
| 3      | 4.4 ± 1.9           | 7.9 ± 1.8           | 11.1 ± 5.0     | 4.2 ± 1.0           | 7.7 ± 1.0           | 0.8 ± 0.6        |
| 4      | 3.8 ± 0.6           | 9.7 ± 0.8           | 4.8 ± 0.6      | 12.3 ± 2.5          | 8.3 ± 2.8           | 4.8 ± 2.9        |
| 5      | 4.7 ± 2.7           | 4.9 ± 1.7           | 7.7 ± 2.3      | 4.4 ± 3.0           | 19.8 ± 2.6          | 12.7 ± 2.9       |
| 6      | 13.0 ± 0.6          | 5.3 ± 0.6           | 3.0 ± 0.5      | 25.1 ± 0.7          | 1.4 ± 1.1           | 6.9 ± 1.1        |
| 7      | 12.2 ± 5.2          | 13.5 ± 5.0          | 19.5 ± 8.1     | 7.3 ± 1.3           | 1.4 ± 0.8           | 1.4 ± 1.0        |
| 8      | 1.0 ± 0.6           | 7.5 ± 0.9           | 4.1 ± 0.4      | 17.4 ± 2.2          | 7.8 ± 2.3           | 16.7 ± 2.8       |

Table A.14: Mean and STD angle error at each joint of the body for SubjectD

| Test # | L Shoulder 1<br>deg | L Shoulder 2<br>deg | L Elbow<br>deg | R Shoulder 1<br>deg | R Shoulder 2<br>deg | R Elbow 2<br>deg |
|--------|---------------------|---------------------|----------------|---------------------|---------------------|------------------|
| 1      | 7.4 ± 1.6           | 4.2 ± 1.0           | 0.6 ± 0.5      | 8.5 ± 1.6           | 8.7 ± 1.0           | 1.6 ± 1.1        |
| 2      | 1.6 ± 1.0           | 7.2 ± 2.0           | 2.4 ± 1.0      | 3.0 ± 2.0           | 8.0 ± 3.7           | 23.3 ± 3.9       |
| 3      | 4.4 ± 2.1           | 2.9 ± 2.1           | 5.6 ± 4.3      | 5.7 ± 1.0           | 8.4 ± 3.0           | 4.2 ± 0.9        |
| 4      | 4.3 ± 2.0           | 4.5 ± 4.5           | 1.0 ± 0.9      | 11.6 ± 5.3          | 12.1 ± 3.1          | 15.0 ± 7.4       |
| 5      | 4.2 ± 1.6           | 1.8 ± 1.0           | 6.6 ± 1.4      | 5.7 ± 2.2           | 7.1 ± 2.6           | 2.7 ± 1.9        |
| 6      | 10.6 ± 0.9          | 3.0 ± 1.6           | 0.3 ± 0.3      | 15.3 ± 0.8          | 13.0 ± 2.1          | 4.2 ± 0.8        |
| 7      | 4.4 ± 2.2           | 4.3 ± 2.3           | 12.8 ± 6.8     | 2.8 ± 1.1           | 11.0 ± 1.4          | 6.2 ± 1.1        |
| 8      | 14.4 ± 1.7          | 3.8 ± 2.0           | 2.8 ± 0.9      | 22.3 ± 3.9          | 21.4 ± 3.0          | 19.0 ± 4.7       |

Table A.15: Mean and STD angle error at each joint of the body for SubjectE